Science of the Total Environment 921 (2024) 171083

Contents lists available at ScienceDirect

Science of the Total Environment

journal homepage: www.elsevier.com/locate/scitotenv

Driving factors of colored dissolved organic matter dynamics across a complex urbanized estuary

Alana Menendez, Maria Tzortziou *

The CUNY Graduate Center, Department of Earth & Environmental Sciences, 365 5th Ave, New York, NY 10016, USA
The City College of New York, The City University of New York, Center for Discovery and Innovation, 85 St Nicholas Terrace, New York, NY 10031, USA

HIGHLIGHTS

- Multi-year and seasonal biogeochemical variability across an urban-estuary gradient
- Clear gradients in DOM amount and quality, in response to urban influence
- Riverine-plume DOC quality impacted by discharge, residence-time and wetland export
- DOC-CDOM uncoupling near NYC urban core was driven by eutrophic conditions
- Fluorescence analysis reveals seasonal dependence in estuarine CDOM transformation

GRAPHICAL ABSTRACT

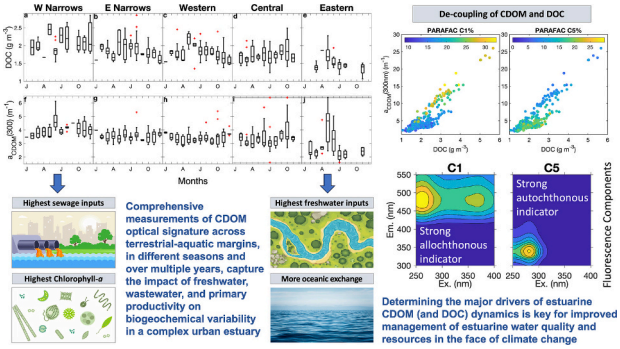

ARTICLE INFO

Editor: Christian Herrera

Keywords:
Carbon cycling
Estuarine
Anthropogenic
Water quality
Urban
DOC

ABSTRACT

The role of estuaries in sourcing and transforming dissolved organic matter - the largest reservoir of organic carbon in the ocean - still presents many unknowns for coastal biogeochemical cycles, and is further complicated by increasing human pressures and a changing climate. Here, we examined the major drivers of colored dissolved organic matter (CDOM) dynamics in Long Island Sound (LIS), a heavily urbanized estuary of National Significance with a storied water quality past. A comprehensive new optical dataset, including measurements of CDOM absorption and fluorescence signatures, was integrated with biological and hydrological measurements to capture the spatiotemporal heterogeneities of LIS, including its urban-to-rural gradient, dynamic river mouths, and blue carbon ecosystems across seasons, following episodic storm events, and over five years. Results reveal longitudinal gradients in both DOM amount and quality. While carbon-rich and humic terrigenous DOM was dominant in the heavily riverine-influenced Central to Eastern LIS, an uncoupling between CDOM absorption (a_{CDOM}) and dissolved organic carbon (DOC) concentration in Western LIS, and a stronger correlation with Chlorophyll-*a*, indicated increased autochthonous CDOM production. Closer to the New York City urban core, a_{CDOM} was highly correlated to turbidity, consistent with increased wastewater influences. Fluorescence PARAFAC analysis provided strong evidence for seasonal processing of CDOM in LIS, related to increased summertime photochemical degradation of humic-like components and shoulder-season microbial processing. Riverine CDOM export was influenced by discharge amount, residence time, and coastal wetlands acting as additional sources of strongly humic and aromatic organic matter. These measurements allowed us to assess how

* Corresponding author.
E-mail address: mtzortziou@ccny.cuny.edu (M. Tzortziou).

https://doi.org/10.1016/j.scitotenv.2024.171083
Received 9 October 2023; Received in revised form 15 February 2024; Accepted 17 February 2024
Available online 20 February 2024

hydrologic, biological, and anthropogenic processes impact DOM dynamics and, subsequently, biogeochemical variability and trophic status in this complex urbanized estuary, with implications for water quality management and policy. Results discussed here are applicable beyond LIS, as urbanized estuaries globally face similar hydrological and anthropogenic forcings.

1. Introduction

Estuaries play an important, yet sometimes mechanistically elusive, role as connectors, transporters, and transformers of biogeochemical constituents across the land-ocean continuum (Bauer et al., 2013; Najjar et al., 2018; Cory and Kling, 2018; Xiao et al., 2022; Regnier et al., 2022). Within these systems, dissolved organic matter (DOM) (defined as <0.2 μm) is a diverse mixture of compounds that impact a wide range of estuarine processes and originate from various – natural and anthropogenic – terrestrial, atmospheric, and marine sources (Vodacek et al., 1997; Stedmon et al., 2000; Raymond and Bauer, 2001; Hernes and Benner, 2003; Boyd and Osburn, 2004; Fellman et al., 2010; Romera-Castillo et al., 2011; Tzortziou et al., 2011; Zhang et al., 2018; Menendez et al., 2022). DOM plays a significant role in aquatic ecosystem functioning because of its role as an energy and nutrient source (D'Andrilli et al., 2019), its control on bacterial abundances and composition (Judd et al., 2006), and the impacts of its colored pool (colored dissolved organic matter, or CDOM) on underwater light availability (Nelson and Siegel, 2002) and temperature (Cory et al., 2015; Kim et al., 2016). The amount and quality (or composition) of CDOM, measured through its optical absorption and fluorescence signatures, when coupled with other environmental variables, reveal information about organic matter provenance, which provides context for carbon cycling regimes (D'Andrilli et al., 2019). The optical properties of CDOM allow for remote detection (Bricaud et al., 1981), which facilitates carbon cycling and water quality insights from CDOM to be attained at more encompassing spatial and temporal scales.

Long Island Sound (LIS) is a complex urban estuary, with about nine million people residing within its watershed and a strong urban-rural gradient driven by New York City on its western boundary. In such a dynamic and heterogeneous landscape, multiple sources and sinks of DOM coexist, and their signatures become integrated. Along with dissolved oxygen (DO), chlorophyll-*a* (Chl-*a*), and water clarity, dissolved organic carbon concentration (DOC) is a key water quality indicator frequently measured by water quality monitoring programs. The nonprofit *Save the Sound* has released water quality report cards across five regions of LIS since 2016 to assess ecological health and the Sound's ability to support aquatic life. The Western Narrows, located closest to the urban core of New York City, has consistently received failing water quality grades, largely due to high nutrient levels from anthropogenic sources resulting in high DOC, low water clarity, and eutrophic conditions that can eventually lead to hypoxia. There have been significant improvements in wastewater treatment technology in and around LIS; notably, from an Environmental Protection Agency mandate, the New York City Department of Environmental Protection reduced nitrogen effluent in its East River plants by 60 % by 2016 from a 1990 baseline. Still, anthropogenic perturbations persist. Almost half (48 %) of the Sound's entire nitrogen budget can be attributed to sewer sources (Vaudrie, 2017). Within the East River, flowing into Western Narrows, 97 % of the nitrogen load is attributed to wastewater treatment plants (Vaudrie, 2017).

In addition to anthropogenic gradients within LIS, river inputs contribute to regional dynamics in estuarine optical properties and biogeochemistry. The Hudson River (Fig. 1), which influences the East River and Western Narrows, is a high CDOM and high biomass endmember within the LIS system (Supino, 2020; Aurin et al., 2010). The Connecticut River, delivering 68 % of LIS freshwater (Vlahos and Whitney, 2017) and 23 % of nitrogen loads adjusted for impact (Save the Sound, 2017), has been identified as a high backscattering endmember due to abundant suspended sediment loads within its plumes (Aurin

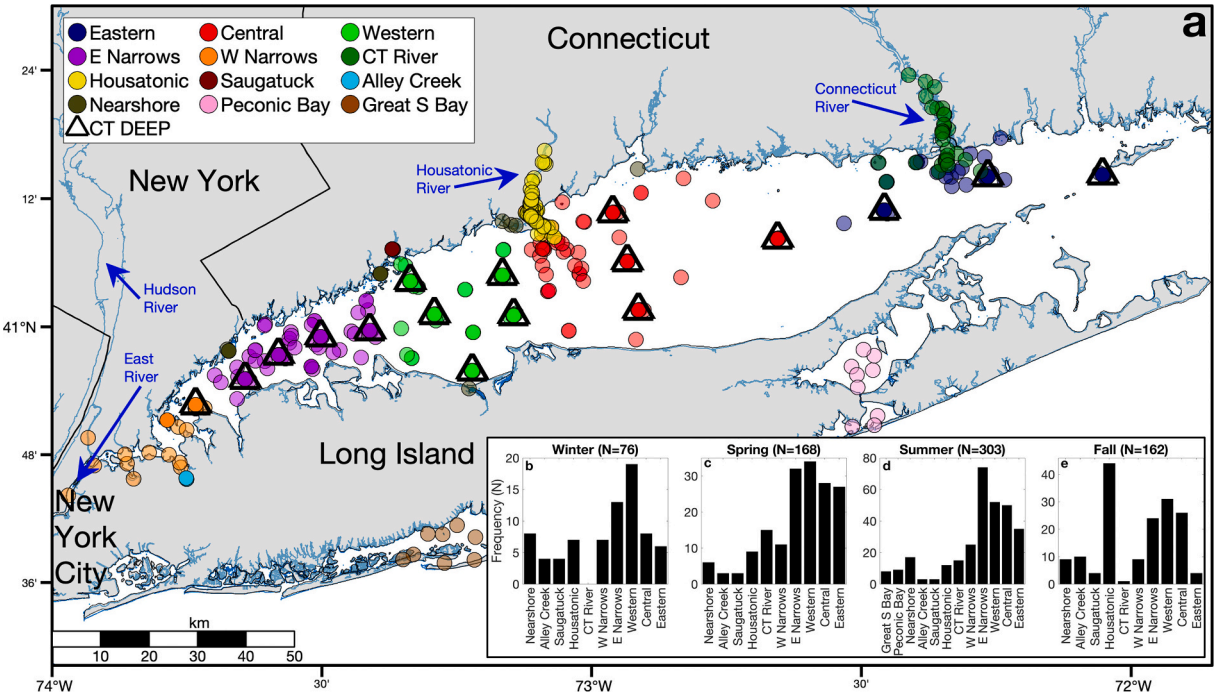

Fig. 1. Locations of measurements collected in Long Island Sound (2017–2022). Triangles indicate sampling sites visited year-round by the Connecticut Department of Energy & Environmental Protection (CT DEEP).

et al., 2010). Another major river in Connecticut, the Housatonic, is responsible for 15 % of LIS freshwater and 17 % of nitrogen loads (Save the Sound, 2017) (adjusted for impact) entering Central LIS. This network of major river systems and many smaller tributaries along the Connecticut shoreline increases riverine loading moving east across LIS, impacting DOM quality. A slight increase in surface water DOC: DON (dissolved organic nitrogen) moving from west to east in 2008–2014 was attributed to more autochthonous material from primary production in Western LIS and higher delivery of terrestrial, humic, and carbon-rich DOM from the Housatonic and Connecticut Rivers moving towards Central and Eastern LIS (Vlahos and Whitney, 2017).

Biogeochemical variability in LIS has been shown to be even greater at seasonal than interannual scales (Gay and O'Donnell, 2009; Vlahos et al., 2020). This is primarily because of the prominent late winter-early spring peak in freshwater from storms and snowmelt that leads to the highest total nitrogen loads in spring and a secondary peak in fall. In Western LIS, spring phytoplankton blooms are supported by the high nitrogen point sources of the East River (Sherman et al., 2023a). Excess nutrient loadings, phytoplankton growth followed by organic matter decomposition, warming temperatures, and enhanced stratification promote the development of recurring, seasonal hypoxia that impacts up to half of the Sound's waters each summer (Valle-Levinson et al., 1995). Increased horizontal exchange, wind mixing, and reduced microbial activity combined with organic matter depletion (Lee and Lwiza, 2008), typically lead to bottom-water DO rebound in late summer and early fall.

In this study, we examined the controls on LIS CDOM variability, specifically the role of rivers and New York City's urban center in sourcing CDOM and the estuary's role in its transformations. With sparse existing CDOM data in LIS and limited biogeochemical and water quality indicators across the Sound's nearshore waters and tributaries, we developed a new, rich dataset that captures the optical signatures of CDOM from diverse pools by sampling at regions of anthropogenic and terrestrial exchange, across the main stem of LIS, during all seasons, and over five years. Such comprehensive in situ knowledge of organic matter dynamics is critical for accurate modeling and satellite remote sensing products of LIS biogeochemical constituents. Results discussed here are applicable beyond LIS, as urbanized estuaries globally face similar hydrological and anthropogenic forcings, and characterizing complex estuarine responses is critical to improving Earth system models (Ward et al., 2020). Finally, enhanced understanding of the main drivers of estuarine CDOM dynamics would allow for better management of estuarine water quality and resources in the face of climate change.

2. Methods

2.1. In situ sample collection

Measurements were collected throughout LIS between September 2017 and June 2022 (collection of 709 unique surface samples), capturing seasonal transitions and a range of environmental conditions (Fig. 1). Main stem sites across the Narrows, Western, Central, and Eastern LIS were sampled in coordination with the Connecticut Department of Energy & Environmental Protection (CT DEEP). CT DEEP has been sampling these locations during monthly to bi-weekly Water Quality and Hypoxia surveys aboard the *R/V Dempsey* since 1991 (https://portal.ct.gov/DEEP/Water/LIS-Monitoring/LIS-Water-Quality-and-Hypoxia-Monitoring-Program-Overview), offering historical context for this newly collected dataset. Sampling in the Housatonic and Connecticut Rivers, and within wetland channels near their river mouths, was done using small charter boats. Five nearshore sites were sampled once a month from November 2020 through December 2021. They were accessed by land, including the Saugatuck River, two locations on the Western Connecticut coastline, from City Island, Bronx, and Alley Creek, Queens, in New York City. Only surface water samples (≤0.5 m depth) were included in this study. Water temperature, salinity, pH, dissolved oxygen, and turbidity were measured using a YSI EXO2 multiparameter sonde. The EXO2 was calibrated and maintained using the standards and protocols delineated in the instrument manual (YSI). Profiles for EXO2 parameters were also analyzed from CT DEEP cruises for surface measurements when samples were collected as part of their water quality monitoring program (https://lisicos.uconn.edu/dep_portal.php). Water samples were collected in clean Nalgene bottles scrubbed, acid-washed, deionized water (DI)-rinsed, and rinsed with sample water. Water samples were kept dark and cold and filtered immediately upon collection (<8 h). When possible, filtering was done within <1 h from collection while onboard the CT DEEP's *R/V Dempsey*.

2.2. Optical analysis

For measurements of CDOM optical (absorption and fluorescence) properties, samples were filtered, first, using a 0.7 μm Whatman GF/F glass microfiber filter and then, a Whatman Nuclepore polycarbonate 0.2 μm filter at low vacuum (Cao et al., 2018). Filtered water was stored in acid-washed and pre-combusted (450 °C) amber glass bottles in the dark at 4 °C for less than a week before further optical analysis.

2.2.1. CDOM absorption

CDOM absorbance measurements were run in triplicate from 240 to 750 nm (at 1-nm bandwidth intervals) on a Cary 300 UV–VIS Spectrophotometer for samples brought to room temperature. We used 5-cm pathlength quartz cuvettes, cleaned thoroughly before analysis, and rinsed with DI and subsequently by water sample between samples, following the protocol of Tzortziou et al. (2008). Sample absorbances were DI-baseline corrected, and DI blanks were subtracted from sample spectra. Potential outliers for triplicate absorbance scans were identified and removed, resulting in quality-controlled mean absorbance spectra for each sample. CDOM absorbance was converted to CDOM absorption using:

$$a_{CDOM}(\lambda) = \frac{2.303A(\lambda)}{l} \quad (1)$$

where $a_{CDOM}(\lambda)$ is CDOM absorption at reference wavelength λ (nm), A is CDOM absorbance at that wavelength, and l is cuvette pathlength in m (0.05 here). The spectral slope of a_{CDOM} (S) was calculated for the range of 275–295 nm ($S_{275–295}$) and 350–400 nm ($S_{350–400}$) by fitting:

$$a_{CDOM}(\lambda) = a_{CDOM}(\lambda_{ref})e^{-S(\lambda-\lambda_{ref})} \quad (2)$$

where λ_{ref} is the reference wavelength, which here is the average wavelength for the spectral range being fitted (285 or 375 nm, respectively), and S is the spectral slope (nm^{-1}) (Helms et al., 2008). The spectral slope ratio (S_R) was calculated as:

$$S_R = \frac{S_{275-295}}{S_{350-400}} \quad (3)$$

(Helms et al., 2008). These metrics of absorption spectral slopes and their ratios were calculated because they have been shown to be good proxies for DOM molecular weight and indicators of DOM source and extent of photochemical or microbial processing (i.e., CDOM quality) in natural waters (Helms et al., 2008; Del Vecchio and Blough, 2002).

2.2.2. CDOM fluorescence

CDOM fluorescence was measured on a Horiba Aqualog Spectrofluorometer at excitation wavelengths of 240–650 nm in 5-nm bands using a 1-cm quartz cuvette and 1-s integration time. Excitation emission matrices (EEMs) were garnered, representing the emission detector's output to the reference detector's signal, after both the emission and reference detector had dark signals subtracted and spectral corrections applied within the Aqualog software. Using the *fdomcorrect* function in the drEEM toolbox (v0.6.0) for Matlab, inner filter corrections were

applied to sample EEMs using sample absorbance averages. A DI EEM blank, run on the same day as a sample, was subsequently subtracted from absorbance-corrected sample EEMs. Raman peaks of DI EEMs were used to convert corrected sample EEMs from raw fluorescence units to Raman Units.

PARAllel FACtor analysis (PARAFAC) was employed to identify underlying fluorescence components within the dataset. Using the Matlab drEEM toolbox, each sample EEM was normalized to its total fluorescence intensity signal, allowing high and low fluorescence samples to have more similar weightings within the model (Murphy et al., 2013). For PARAFAC, 25 samples were identified as outliers and excluded from the model, which left 735 unique sample EEMs remaining. PARAFAC modeled results were validated using split-half analysis (four splits with six combinations and three validations, 'S4C6T3'), and through analysis of sample residuals (Murphy et al., 2013).

PARAFAC component model values were converted to F_{max} in Raman Units by multiplying each sample's modeled component fluorescence intensities by the overall sample fluorescence intensity. Percentage F_{max} of each sample component was found by dividing the F_{max} of a given sample component by the total F_{max} for all components within that sample, multiplied by 100. This is discussed moving forward as component percentage (C_i%) and represents each component's contribution to total sample fluorescence.

$$C_i\% = \frac{C_i F_{max}}{\sum_{i=1}^{7} C_i F_{max}} * 100 \quad (4)$$

2.3. DOC analysis

Samples for measurements of DOC concentrations, [DOC], were filtered and stored identically to filtrate for CDOM, except DOC samples were in duplicate bottles and acidified to pH ~2–3 using 10 % HCl immediately after filtering. [DOC] was measured in duplicate with a Shimadzu TOC-V (Total Organic Carbon) Autoanalyzer. Samples for DOC were flagged and excluded from analysis if the coefficient of variation between duplicates was >15 %. A total of 505 samples were included in our analysis. DOC-specific CDOM absorption ($a^*_{CDOM}(300)$ ($m^2\ g^{-1}$)) was calculated as the ratio of a_{CDOM} amount at 300 nm ($a_{CDOM}(300)$ (m^{-1}) to [DOC] (g m^{-3})). Previous studies have shown that a^*_{CDOM} is a good proxy for DOM composition, increasing with increasing molecular weight and aromaticity (e.g., Del Vecchio and Blough, 2004; Tzortziou et al., 2008).

2.4. Chlorophyll-a analysis

Samples for chlorophyll-*a* (Chl-*a*) measurements were filtered simultaneously as CDOM and DOC, in duplicate, using 0.7 μm Whatman GF/F glass microfiber filters. Filters were stored between −20 and −80 °C. Chl-*a* was extracted from its filters in 90 % acetone and measured fluorometrically in duplicate using a Turner Designs Trilogy fluorometer. Samples for Chl-*a* were flagged and excluded from analysis if the coefficient of variation between duplicates was >15 %. A total of 552 samples were included in our analysis.

2.5. Discharge and precipitation analysis

United States Geological Survey tidally filtered discharge data from the Connecticut River at Middle Haddam, CT (site 01193050, Lat = 41°32′30″, Lon = −72°33′13″) and discharge data from the Housatonic River at Stevenson, CT (site 01205500, Lat = 41°23′01.69″, Lon = −73°09′59.90″) were compiled and converted from their native sampling frequency ($ft^3\ s^{-1}$ discharge averages at hourly and 15-minute sampling intervals, respectively) to $m^3\ s^{-1}$ mean daily discharge for the project duration. Mean daily discharges for both rivers were extracted on days of sample collection.

We used meteorological data from the National Oceanographic and Atmospheric Administration's Applied Climate Information System (ACIS), following the methodology of Sherman et al. (2023a). Daily precipitation data gridded to 5 × 5 km resolution was interpolated from the National Weather Service Cooperative observer network by the Northeast Regional Climate Center, which was chosen to align with meteorological LIS reports produced by CT DEEP. Regional averages of daily precipitation data were generated to capture precipitation impacts on LIS across its spatial domain. For sampling date, we calculated daily precipitation summations for the preceding seven days to account for possible lags of precipitation impacts reaching the estuary; this preceding seven-day summation is referred to as 'precipitation' moving forward.

2.6. Regional binning

Regions of LIS were defined using the boundaries of the *Save the Sound* water quality report card, which demarcates Western Narrows (WN), Eastern Narrows (EN), Western (WLIS), Central (CLIS), and Eastern LIS (ELIS) (Fig. 1). A second filtering using a salinity threshold of 24 was applied to distinguish between Housatonic River and CLIS samples, and between Connecticut River and ELIS samples, where tidal phase and discharge extremity can dictate what water is sampled surrounding the dynamic river mouths. This salinity threshold was chosen based on visual clustering when examining $a_{CDOM}(300)$ versus salinity for the entire LIS dataset. With this salinity threshold, higher salinity samples were characterized as CLIS or ELIS, and lower salinity (brackish) samples were classified as riverine. Water samples taken from shore along the CT coastline were classified as Nearshore.

2.7. Correlation, PCA, and multilinear regression analysis

Pearson correlation coefficients (r) were calculated between selected optical, biogeochemical, and physicochemical variables subject to specific regional, temporal, or salinity binning, using standardized data (standard scaler) and Matlab's *corrcoef* function. Principal component coefficients (loadings) and principal component scores for data observations were calculated on the standardized dataset using Matlab's Principal Component Analysis (PCA) *pca* function. [DOC] and $a_{CDOM}(300)$ were modeled using Matlab's *stepwiselm* function, which successively takes in and out predictors based on statistical significance (we used p-value ≤ 0.05 for removal). This was done using data from all regions, months, and years together. [DOC] was modeled with the possible predictor variables of Chl-*a*, salinity, pH, dissolved oxygen, water temperature, turbidity, Connecticut River discharge, Housatonic River discharge, and precipitation. We modeled $a_{CDOM}(300)$ from the complete list of predictor variables above, with the addition of [DOC]. Predictor variables were standardized prior to input to *stepwiselm*.

3. Results and discussion

3.1. Spatiotemporal dynamics in CDOM across the main stem of the Sound

CDOM absorption showed strong longitudinal trends across the LIS main stem, with $a_{CDOM}(300)$ decreasing by ~40 %, from 4.15 m^{-1} in WN to 2.53 m^{-1} in ELIS (Fig. 3f–j). In WN, $a_{CDOM}(300)$ remained within a narrow and overall elevated range of ~3.3–5.0 m^{-1} (Fig. 3f) across seasons, consistent with failing water quality grades in this region due to intense anthropogenic pollution, including continuous pulses of wastewater (Save the Sound, 2022). In addition to CDOM absorption magnitude, the spectral signature of CDOM also showed considerable spatial gradients across the Sound. $S_{275–295}$ increased from 0.0204 nm^{-1} in WN to 0.0213 nm^{-1} in CLIS yet decreased again to 0.0206 nm^{-1} in ELIS, capturing the influence of freshwater inputs from the Connecticut River (Fig. 3k–o). High variability in a^*_{CDOM} and $S_{275–295}$, both proxies for

DOM molecular weight and aromaticity, were observed in CLIS and ELIS (Fig. 3n, o, s, t), indicating the coupled influence of freshwater inputs from the two largest LIS rivers as well as photochemical and microbial transformations (Tzortziou et al., 2008; Helms et al., 2008). An extensive range in $a_{CDOM}(300)$ (Fig. 3j) and $S_{275–295}$ (Fig. 3o) was found in ELIS, highlighting the additional influence and complex mixing of marine water from the Atlantic Ocean (with ocean waters characterized by lower $a_{CDOM}(300)$ and higher $S_{275–295}$ (Yamashita et al., 2013)).

Similar to CDOM, DOC also showed strong longitudinal trends across the LIS main stem, decreasing by ~25 %, from 1.93 g m^{-3} in WN to 1.47 g m^{-3} in ELIS (Fig. 3a–e). Strong relationships between CDOM absorption and DOC concentration have been previously documented across coastal waters (e.g., Mannino et al., 2008; Vantrepotte et al., 2015; Joshi et al., 2017; Juhls et al., 2019; Sanwlani et al., 2022). Yet, in inland and estuarine systems, the DOC: CDOM relationship varies due to the complex interplay of multiple biogeochemical, physicochemical, and hydrological processes that impact the source and composition of DOC (e.g., Del Vecchio and Blough, 2002; Fichot and Benner, 2011; Stedmon and Nelson, 2015). Across the main stem of the Sound, $a_{CDOM}(300)$ and [DOC] were strongly coupled in ELIS ($r = 0.90$; $p < 0.001$) and moderately correlated in CLIS ($r = 0.45$; $p < 0.01$), with strong negative correlation between $a_{CDOM}(300)$ and salinity (r of −0.8 to −0.84; $p < 0.001$) (Fig. S1) indicating the dominant role of freshwater inputs of C-rich and strongly colored DOM in driving biogeochemical variability. Yet, $a_{CDOM}(300)$ and [DOC] were not significantly correlated in WN, EN, or WLIS, and in these regions there was a decrease in the correlation between CDOM and salinity (r of −0.42 to −0.56; all with $p < 0.05$), and a significant correlation between $a_{CDOM}(300)$ and Chl-*a* in EN and WLIS (r of 0.33–0.37; $p < 0.01$) (Fig. S1). Higher Chl-*a* concentrations in WN (7.15 mg m^{-3} median) compared to ELIS (2.76 mg m^{-3} median) indicate a more important role of autochthonous production of organic carbon that contributes to the regional decoupling of $a_{CDOM}(300)$ and [DOC] in the western regions of LIS. These results also agree with the increase in surface water DOC: DON moving from west to east reported in previous studies, attributed to more autochthonous material from primary production in Western LIS (Vlahos and Whitney, 2017). In addition to biological activity, wastewater impacts nutrient dynamics in Western LIS (Humphries et al., 2023). In Western Narrows, $a_{CDOM}(300)$ was

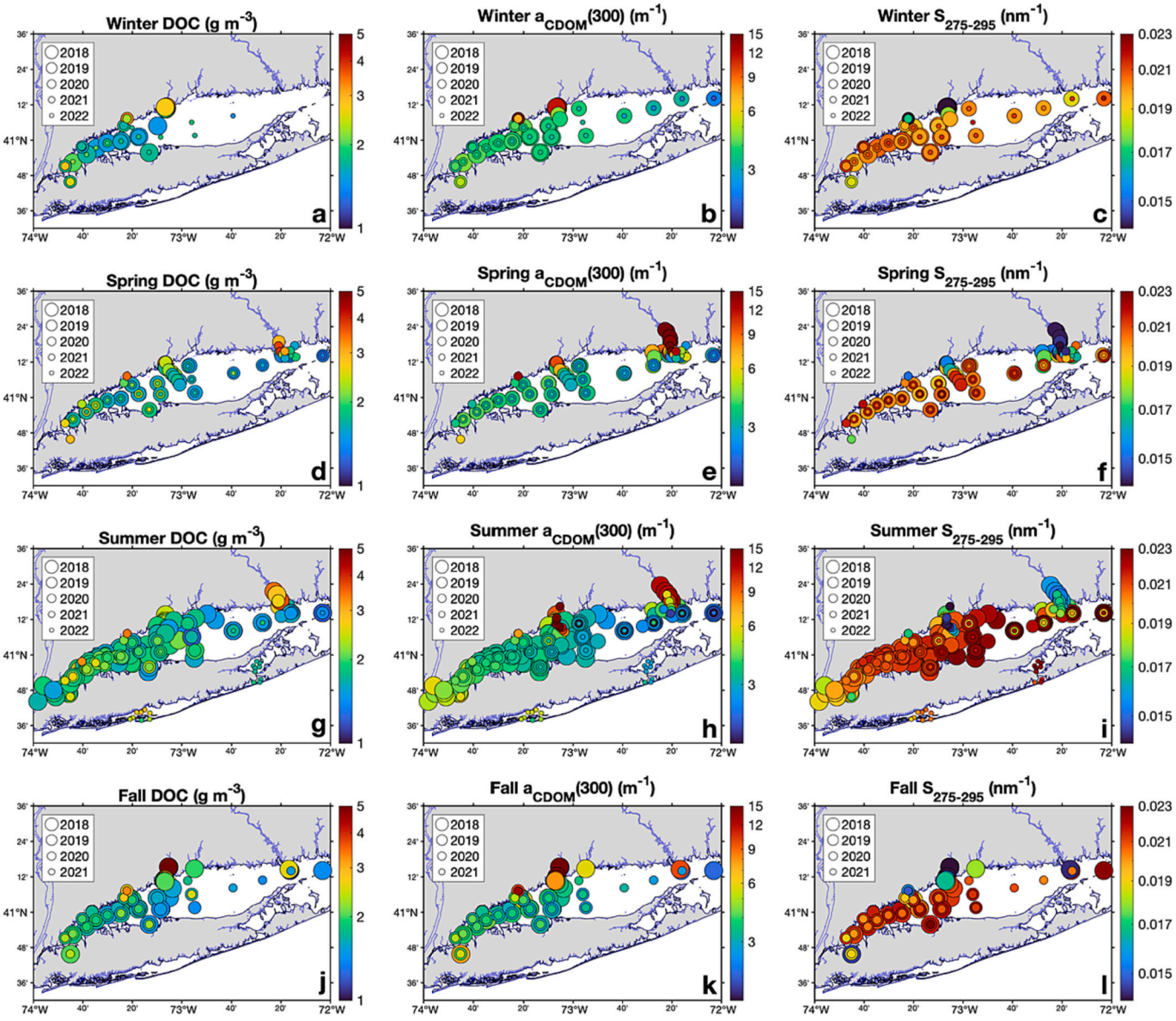

Fig. 2. Surface [DOC] (a, d, g, j), surface $a_{CDOM}(300)$ (b, e, h, k), and surface $S_{275–295}$ (c, f, i, l) collected in and around LIS waters during this study by season. The sizes of circles illustrate interannual variability.

strongly correlated to turbidity ($r = 0.75$; $p < 0.001$) (Fig. S1). Changes in turbidity were previously shown to be linked to wastewater effluent inputs in the New York Harbor Upper Bay (Sherman et al., 2023a). Bordering New York City, WN is directly impacted by the East River (Blumberg and Pritchard, 1997), where there is high wastewater loading. A strong positive correlation was also found between $a_{CDOM}(300)$ and total precipitation in Alley Creek ($r = 0.87$; $p < 0.01$) (Fig. S1), highlighting the strong influence of wetland and sewage DOM inputs, both sources previously shown to result in disproportionate export of strongly absorbing organic matter under flooding conditions (D'Sa et al., 2023; Cao and Tzortziou, 2021; Ayad et al., 2020).

Beyond their influence on CDOM spatial variability, hydrological processes, human activity, and biological production are expected to impact temporal transitions in CDOM across the main stem of the Sound. Interestingly, seasonal variability is larger than interannual variability for total nitrogen inputs in LIS, typically showing maxima during spring runoff and snowmelt, a decrease in summer, and an increase again by fall (Vlahos et al., 2020). Within mainstem LIS, seasonal transitions were depicted in CDOM quality, as captured by changes in $S_{275–295}$ (Fig. 2c, f, I, l; Fig. 3k–o) and a^*_{CDOM} (Fig. 3p–t). The highest $S_{275–295}$ and lowest a^*_{CDOM} were consistently observed in summer, mainly in July, particularly in the Eastern Narrows, Western, and Central LIS (Fig. 3l, m, n, q, s). These regions are less directly impacted by human activity, compared to the Western Narrows, or episodic discharge events, compared to Eastern LIS, both processes often masking seasonal cycles. Higher $S_{275–295}$ and lower a^*_{CDOM} during summer are both indicative of increased photochemical degradation (Helms et al., 2008; Fichot and Benner, 2012) and/or biological production (Nelson et al., 2004; Steinberg et al., 2004). Biological processes such as grazing and microbial activity in early summer, following intense spring phytoplankton blooms, could be responsible for the accumulation of semi-labile, less-absorbing DOM (Mannino et al., 2008), contributing to the decrease in a^*_{CDOM} and increase in $S_{275–295}$ that we observed in May and June in EN and WLIS (Fig. 3b, c, g, h, q, r).

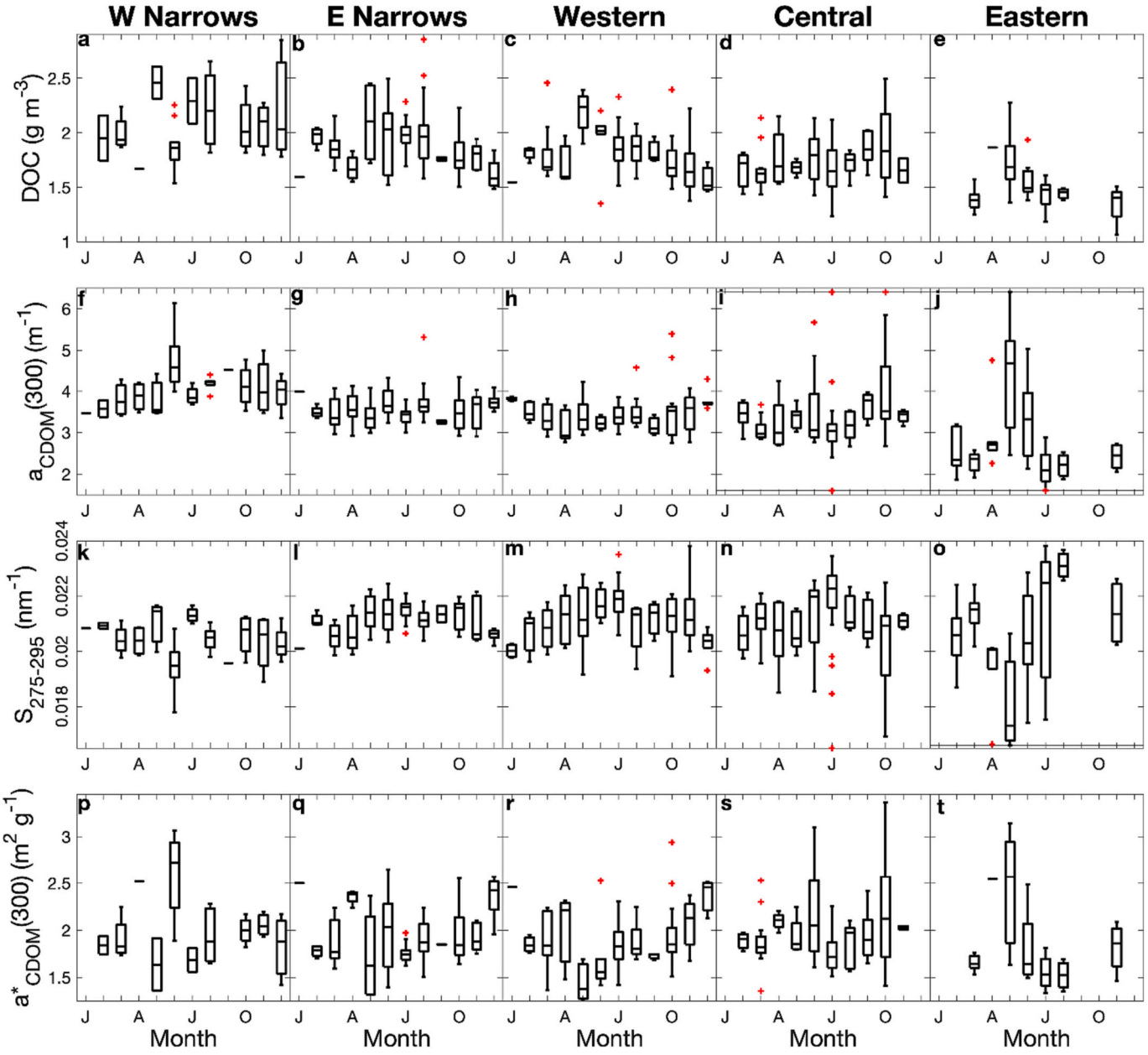

Fig. 3. Monthly boxplot distributions (depicting median, 25th percentile, 75th percentile, and whiskers extending to ±2.7 σ, and outliers in red) of [DOC], $a_{CDOM}(300)$, $S_{275–295}$, and $a^*_{CDOM}(300)$ for WN, EN, WLIS, CLIS, and ELIS.

Interestingly, $a_{CDOM}(300)$ did not show strong seasonality in EN and WLIS (Fig. 3g, h). However, we found seasonal changes in the magnitude and direction of correlations between a_{CDOM}, hydrological forcing, and Chl-*a* concentrations in EN and WLIS that provide insight into the observed seasonality in CDOM quality (i.e., S and a^*_{CDOM}). In winter, hydrologic conditions were highly correlated to $a_{CDOM}(300)$, both in terms of total precipitation ($r = 0.79$, $p < 0.01$ for EN; $r = 0.97$, $p < 0.001$ for WLIS) as well as Connecticut River discharge ($r = 0.80$, $p < 0.01$ for EN; $r = 0.92$, $p < 0.01$ for WLIS) and Housatonic River discharge ($r = 0.82$, $p < 0.01$ for EN; $r = 0.97$, $p < 0.001$ for WLIS). These results suggest that wintertime $a_{CDOM}(300)$ is heavily allochthonous in these regions, driven by winter storms and predominantly Northerly winds that favor extensive river plumes in LIS (Cao and Tzortziou, 2024). Besides the Connecticut and Housatonic Rivers that, together, account for 83 % of freshwater entering LIS (Save the Sound, 2017), EN and WLIS directly experience freshwater inflows from the Byram, Mianus, Rippowam, Norwalk, and Saugatuck Rivers. These smaller rivers have been demonstrated to have faster freshwater delivery to the coast after storm events than larger neighboring river systems (Deignan-Schmidt and Whitney, 2017), which may make these LIS regions particularly sensitive to allochthonous delivery of high-CDOM waters after seasonal storms. Chl-*a* concentration was the strongest predictor of WLIS $a_{CDOM}(300)$ in spring ($r = 0.78$, $p < 0.001$), and of both EN and WLIS $a_{CDOM}(300)$ in summer ($r = 0.55$, $p < 0.001$ and $r = 0.62$, $p < 0.001$, respectively), indicating dominant autochthonous production and seasonal shifts in CDOM composition as captured by the CDOM spectral signature (i.e., a^*_{CDOM} and $S_{275–295}$).

3.2. Further insights from fluorescence analysis

PARAFAC modeling resulted in seven components for our dataset that explained ~99.89 % of the variability in the DOM fluorescence signal, with component excitation and emission maximums and classifications shown in Table 1. These components were compared to the OpenFluor (Murphy et al., 2014) database and literature matches. Components 1 to 7 (C1–C7) had 100, 44, 36, 18, 89, 23, and 6 OpenFluor matches, respectively. Based on these results, we designated our seven modeled components as long-wavelength humic (C1), visible humic (C2), degraded humic (C3), marine/UV humic (C3), tryptophan-like (Trp) (C5), tyrosine-like (Tyr) (C6), and phenolic compound (C7) (Table 1). Notably, 5-out-of-25 PARAFAC surface samples identified as outliers for the model were from Alley Creek. Their anomalous distinct fluorescence peaks indicate that the samples with the strongest wastewater signals were excluded from this analysis for PARAFAC to validate.

3.2.1. Humic-like fluorescent components

Humic-like components C1 and C2 had a combined contribution of 19–60 % to total fluorescence signal across LIS and were highly correlated – suggesting similar sources and sinks – both in the brackish and higher salinity LIS waters ($r = 0.94$ and 0.91, respectively; $p < 0.001$; Fig. 4). These fluorescence components have been associated with terrestrial material (Coble, 1996; Stedmon et al., 2003; Murphy et al., 2008), with C1 corresponding more likely to higher molecular weight DOM than C2 based on the longer wavelength emission (Table 1; Fig. 5a, b) (Stedmon et al., 2003; McKnight et al., 2001).

C1 and C2 had the highest percent contribution in samples collected from the Housatonic and Connecticut Rivers (Fig. 5o, p). They showed similar seasonal variability, with the lowest relative contributions in July and August and the highest in January and December (Fig. 5h, i). These patterns are consistent with lower terrigenous DOM inputs in summer (due to lower river discharge; (Cao and Tzortziou, 2024)) and the highest summertime loss of humic DOM from photochemical degradation (Tzortziou et al., 2007). C1% and C2% showed strong negative correlations with $S_{275–295}$ in brackish waters ($r = -0.81$ and -0.87, respectively; $p < 0.001$; Fig. 4a), supporting riverine delivery of terrestrial material that is less degraded or altered (Helms et al., 2008). In the higher salinity sample pool (>24), C1% and C2% were still correlated to $S_{275–295}$ ($p < 0.001$; Fig. 4b), highlighting that $S_{275–295}$ is a sensitive indicator of terrigenous influence in LIS waters that have undergone mixing (for comparison, $a_{CDOM}(300)$ had substantially weaker marine subset C1% and C2% correlations; $p < 0.01$).

Humic-like C3 was overall the most ubiquitous and prominent component contributing to total fluorescence (Fig. 5j, q, x), with a median sample contribution of 20 %. Classically defined as peak A (Coble, 1996), C3 has been characterized as humic-like material, but despite terrestrial precursors, it has been shown to persist into the estuarine realm (Stedmon and Markager, 2005). Interannually, C3 fluorescence contributions were reduced in 2020 (Fig. 5x), the year of lowest riverine freshwater discharge in this study (Fig. S2). Previous studies suggest that C3 is more prevalent in warmer months (Stedmon and Markager, 2005; Kothawala et al., 2014), and may be a photoproduct of terrestrial DOM resistant to further photodegradation (Stedmon et al., 2007; Stedmon and Markager, 2005). This is consistent with our findings of increased contributions of C3 to the fluorescence pool in summer, particularly in June and September (Fig. 5j). C3 has also been found to be resistant to biodegradation (Stubbins et al., 2014; Ishii and Boyer, 2012). Interestingly, C3% in LIS brackish waters (<24) showed a positive correlation with $S_{350–400}$ ($p < 0.001$; Fig. 4a), which has been linked to microbial degradation (Helms et al., 2008; Grunert et al., 2021). Grunert et al. (2021) found that both photochemically and biologically labile molecules can contribute to this component and that there is competitive degradation by sunlight and microbes of the precursor compounds that produce C3.

Marine/UV humic-like peak C4 has similar excitation and emission wavelengths to the classically defined M peak (Coble, 1996), characterized as less aromatic and of lower molecular weight than C1, C2, and C3 (Fellman et al., 2010). Marine humic fluorophores have been demonstrated to be exudated during the exponential growth phase of a phytoplankton bloom (Romera-Castillo et al., 2009) and attributed to the degradation of tryptophan-like DOM freshly produced from a bloom (Yamashita and Tanoue, 2004). Similar peaks have also been associated with wastewater and terrestrial sources (Murphy et al., 2008; Fellman et al., 2010). In LIS brackish waters, C4% was positively correlated to $S_{275–295}$ ($p < 0.05$) and negatively correlated to Connecticut River discharge ($p < 0.05$), all indicators of autochthonous origin (Fig. 4a). Spatially, C4 had the highest contribution in Western Narrows (Fig. 5r), characterized by high Chl-*a* concentrations and intense microbial processing, further supporting a C4 relationship to biological production.

Omori et al. (2020) explored the diurnal cycling of marine humic DOM, showing microbial production of humic DOM at night and simultaneous photobleaching (degradation) and microbial production during the day, described as an equilibrium. C4% showed a negative correlation with the humic component C1% ($p < 0.05$) and was not significantly correlated to C2% in the brackish LIS river plumes (Fig. 4a), but had positive correlations to C1% and C2% in the main stem ($p < 0.001$; Fig. 4b), consistent with previous studies showing the production of humic-like DOM during microbial processing, particularly after

Table 1
Characterizations of PARAFAC components with excitation (Ex.) and emission (Em.) maximum wavelengths. Secondary excitation peaks are shown in parentheses.

Component	Ex. max λ (nm)	Em. max λ (nm)	Characterization
C1	260 (365)	482	Long-wavelength humic (red-shifted)
C2	250 (330)	422	Visible humic (blue-shifted)
C3	<250	436	Degraded humic byproduct
C4	305 (<250)	380	Marine/UV humic
C5	280	340	Free tryptophan-like
C6	270	300	Tyrosine-like
C7	255	330	Phenolic compound

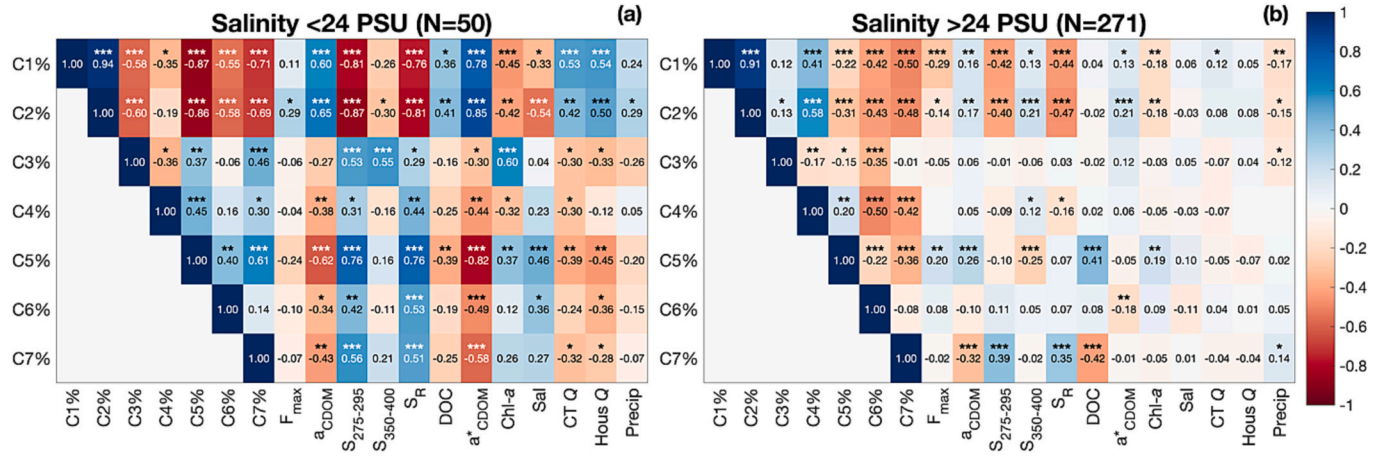

Fig. 4. Heatmaps show Pearson correlation coefficients for comparisons between PARAFAC component fluorescence contributions and optical, biogeochemical, and ancillary parameters. The data presented is separated into two salinity ranges with brackish waters shown on the left (<24) (a) and main stem waters shown on the right (>24) (b). Asterisks correspond to significance levels, with *** = $p < 0.001$, ** = $p < 0.01$, and * = $p < 0.05$.

photobleaching (Mann et al., 2012; Grunert et al., 2021). Across PCA Dimension 2 (PC2) (explaining 12.1 % of variability), we found strong correlations between C4% and $S_{350–400}$ (known to increase with microbial activity) (Table S1), particularly in March (Fig. 6b) that correspond to typical post-phytoplankton bloom periods in LIS (Sherman et al., 2023b; Rice and Stewart, 2013). Interestingly, Chl-*a* and C4 were negatively correlated in brackish waters ($p < 0.05$) and not correlated in the marine waters (Fig. 4; Fig. 6a–b), potentially due to the time lag between the occurrence of a bloom and associated fluorescent DOM production from viral lysis (Shimotori et al., 2009). In LIS Narrows, bacterial biomass increased from July through August with temperature, and bacterial net production peaks lagged Chl-*a* by about a week (Anderson and Taylor, 2001). Increased daylight in summer, leading to greater photochemical degradation than microbial production of C4, could help explain why the maximum marine humic C4% does not occur in summer (in sync with potentially highest bacterial biomass) (Omori et al., 2020).

In our analysis, 5-out-of-25 EEMs flagged as outliers in PARAFAC analysis were Eastern Narrows samples from August 26, 2020 (Fig. S3), that all contained prominent fluorescence near the region of the classically defined humic peak D (reported at Ex. 390 nm and Em. 509 nm), associated with soil fulvic acid (Stedmon et al., 2003). However, soil fulvic acid inputs were inconsistent with the East Narrows location of these samples, which were subject to little soil/terrestrial influence at the sampling time. Instead, whole water phytoplankton analysis (preserved with Lugol's iodine solution) from FlowCam imagery suggests a link to harmful algal bloom conditions. FlowCam analysis (data not shown here) indicated that these five samples contained a high number of dinoflagellates, including possibly *Akashiwo sanguinea*, of which blooms have coincided with high stratification (Menden-Deuer and Montalbano, 2015) and eutrophic conditions in Eastern Narrows in late August. While the toxicity of *Akashiwo sanguinea* is unclear, it has been linked to seabird, microzooplankton, and larvae deaths (Menden-Deuer and Montalbano, 2015). Fukuzaki et al. (2014) have detected humic-like fluorescence DOM peaks (Ex. 370 nm, Em. 450–470 nm) associated with exudates from *Heterosigma akashiwo*, not directly related to *Akashiwo sanguinea*, but another species of harmful algae, and emphasize this unique finding considering this fluorescence region is traditionally associated with terrestrial substances.

3.2.2. *Protein-like fluorescent components*

Phytoplankton and bacteria have been shown to produce protein-like fluorophores (e.g., Determann et al., 1998; Yamashita and Tanoue, 2003; Stedmon and Markager, 2005). In the Sound, C5 (consistent with free tryptophan (Trp) in literature; Stedmon and Nelson, 2015) was the protein-like component with the greatest median percent contribution (16 %) to sample fluorescence (Fig. 5l, s, z) and the only component positively correlated to Chl-*a* concentration, both in the LIS mainstem and the nearshore/brackish waters ($p < 0.01$) (Fig. 4). Spatially, C5 had the greatest contribution to total fluorescence in the most productive WN region (Fig. 5s). Although C5% was negatively correlated with [DOC] in nearshore brackish LIS waters ($p < 0.01$) (where the signal from terrigenous DOC would dominate) (Fig. 4a), it was the only component that had a substantial positive correlation to [DOC] in the higher salinity sample pool ($p < 0.001$) (Fig. 4b), suggesting that C5 is a good indicator for marine production of DOC in LIS.

Component 6, consistent with tyrosine-like (Tyr) fluorescence in literature, had the most considerable variability in percent contribution to total fluorescence (ranging from 0 to 40 %) with a median contribution of 8.7 % (Fig. 5m, t, aa). C6 did not show any apparent seasonal or interannual variability, potentially due to the fluorescence intensity of tyrosine being strongly affected by its free-or-bound status with proteins. Determann et al. (1998) found that free-Trp and free-Tyr had similar emission fluorescence efficiencies. However, when bound to proteins, Trp had 3–5 times higher intensity than Tyr due to a transfer of energy from Tyr emission to the excitation of Trp (i.e., Tyr is quenched) (Lakowicz, 2006; Aiken, 2014). Unlike the linkages between [DOC] and the other two protein-like components in the LIS main stem (with C5 corresponding to DOC production and C7 to DOC loss), C6 was not significantly correlated to [DOC] (Fig. 4b). The C6 Tyr-like peak has been described as indicative of more degraded peptide material than the Trp-like C5 peak (Fellman et al., 2008), consistent with the higher contributions of C6% in the less productive eastern LIS (Fig. 5t).

Component 7 had spectral characteristics similar to tryptophan-like fluorescence but slightly blue-shifted, corresponding spectrally to phenolic compounds from gallic acid (Wünsch et al., 2015) and condensed tannins from red mangrove leaves (Maie et al., 2007). Free phenolic compounds in seawaters could have multiple sources, including phytoplankton exudates, degradation of lignin compounds, or atmospheric sources, such as biomass burning (Zangrando et al., 2019). Scully et al. (2004) suggested that the low molecular weight fraction of polyphenols exported from mangroves and seagrass can be removed through photooxidation by reactive oxygen species, with photochemical half-lives of 9–22 h. In LIS, C7% had the highest contribution in July–August, was positively correlated to $S_{275–295}$ in marine waters ($p < 0.001$), and was the only component in the higher salinity sample pool to correlate to a loss of $a_{CDOM}(300)$ ($p < 0.001$) and an even greater loss of DOC ($p < 0.001$) (Fig. 4b), suggesting degradation of autochthonous DOM as a possible source, especially in summer (Scully et al., 2004). This is consistent with PC5, explaining 6.9 % of variability, correlating

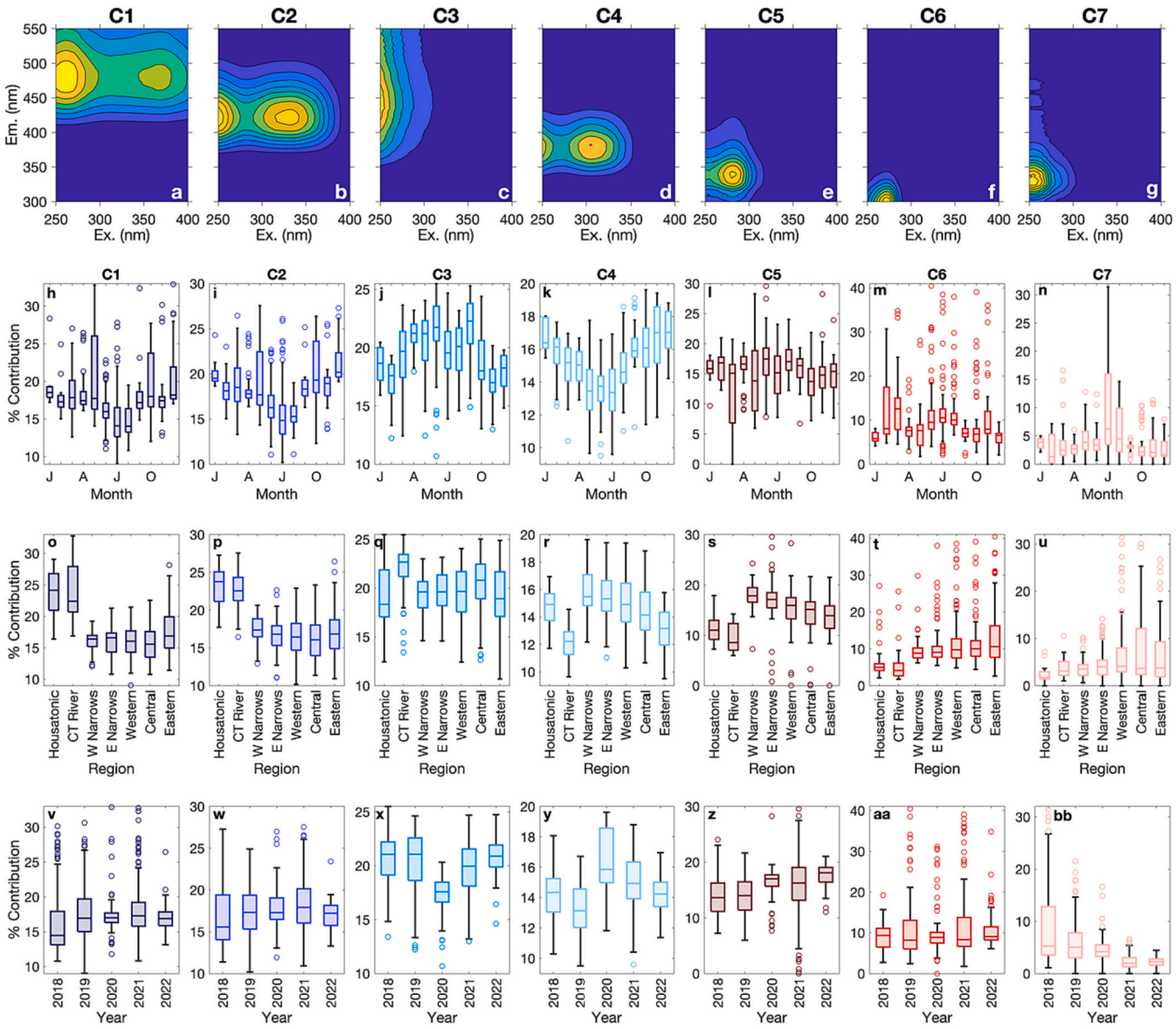

Fig. 5. Fingerprints of excitation (x-axis) and emission (y-axis) intensities for the seven fluorescence components identified from the PARAFAC model (a–g), along with boxplots of monthly (h–n), regional (o–u), and interannual (v–bb) component percent contributions to total sample fluorescence, for all samples (boxplots depict median, 25th percentile, 75th percentile, whiskers extend to ±2.7 σ, and outliers are shown with circles).

positively to Chl-*a* (loading of 0.36), C5% (loading of 0.34), and [DOC] (loading of 0.23), but correlating negatively to C7% (loading of −0.36) (Table S1).

3.3. DOM dynamics in LIS rivers and plumes

Compared to mainstem LIS, almost twofold higher DOC concentrations were consistently measured in the Housatonic and Connecticut rivers, with median values of 3.06 g m^{-3} ($N = 53$) and 2.97 g m^{-3} ($N = 11$), respectively. Even more pronounced was the riverine impact on CDOM absorption, with both rivers having median $a_{CDOM}(300)$ 3–4.5 times the main stem values (Housatonic River 11.68 m^{-1} ($N = 71$) and Connecticut River 12.15 m^{-1} ($N = 30$)) and maxima 2.5–7 times higher than main stem regional maxima in $a_{CDOM}(300)$ (Housatonic River 37.32 m^{-1} and Connecticut River 20.26 m^{-1}). $S_{275–295}$ showed steep differences between main stem basins (median of 0.020–0.021 nm^{-1}, Fig. 3k–o) and river sites (0.0150–0.0153 nm^{-1}). Both major rivers had $S_{275–295}$ values reaching as low as 0.0127 nm^{-1}.

Rivers have been shown to have a significant influence on LIS carbon budgets (Vlahos and Whitney, 2017), nitrogen fluxes (Vlahos et al., 2020), and optical complexity (Aurin et al., 2010). Yet, their impact on DOM quality and distribution across the LIS urban-to-rural and freshwater-to-marine continuum has not been thoroughly examined. Our high-resolution measurements along the Housatonic and Connecticut River plumes allowed us to assess how this allochthonous CDOM is mixed as it enters LIS under conditions of varying discharge. Positive deviations from lines representing conservative mixing with salinity (Fig. 7) indicated additional sources of strongly colored DOM in regions dominated by extensive brackish wetlands in the Connecticut and Housatonic River mouths. Wetlands have been shown to be strong sources of aromatic, humic, photoreactive, and optically distinctive (higher a^*_{CDOM} and lower $S_{275–295}$) CDOM across a range of estuarine and coastal systems (Tzortziou et al., 2008; Logozzo et al., 2021; Menendez et al., 2022). We found that in the wetland-dominated river mouths, $a^*_{CDOM}(300)$, C1, and C2 F_{max} were higher than expected based on conservative mixing, suggesting additional input of humic and strongly aromatic DOM. These instances are depicted with the dark green shading in Fig. 7 (a, b, g, h) for the lower discharge transects (June

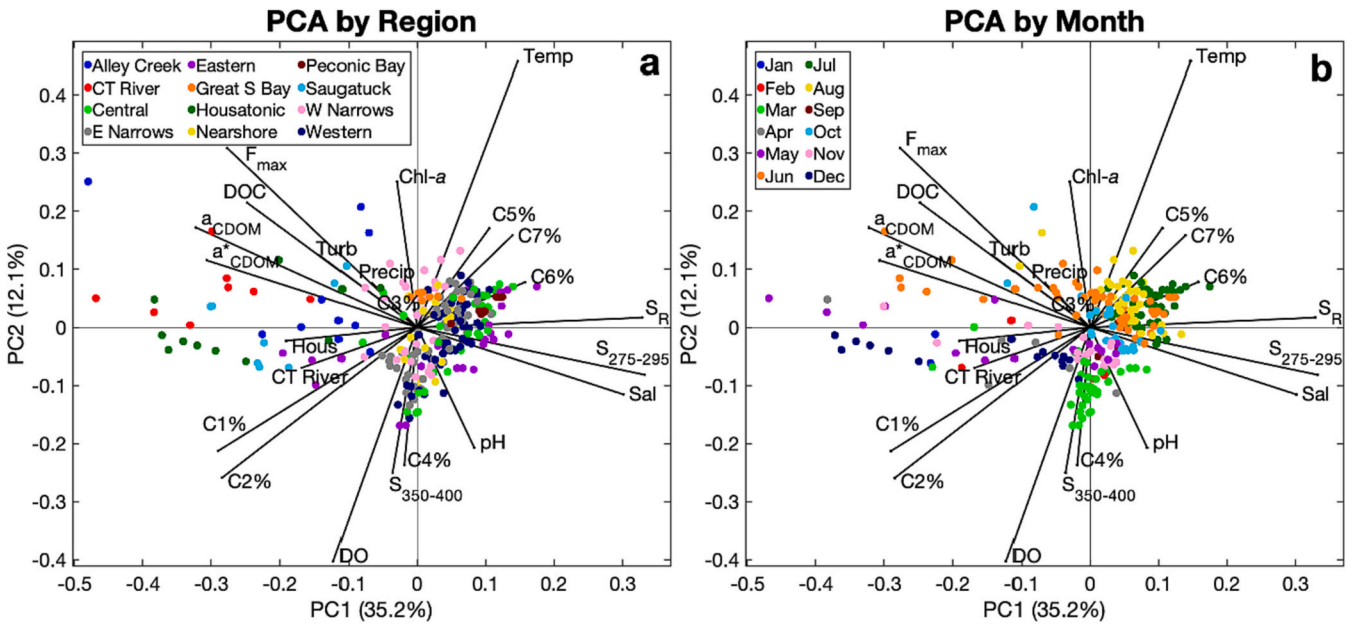

Fig. 6. Principal Component Analysis (PCA) for dimension 2 (PC2) versus dimension 1 (PC1) along with the explained variability captured with each principal component. Variable loadings are shown in black lines and sample scores are colored by region (a) and month (b). The subset of data (with no missing parameters) for PCA analysis had $N = 277$.

27, 2018, Wheeler Marsh at the Housatonic mouth and June 8, 2018, Lord Cove Marsh at the Connecticut River mouth). Interestingly, these samples show not just additions of terrestrial-associated fluorescence components (C1 and C2) but also consistent additions of C3, C4, and C5 for all four of these wetland channel samples, indicating photo-biogeochemical transformation and/or riverine biological production during lower flow periods. For these two low-discharge June transects, Chl-*a* was found to be higher in the river than estuary endmember, with concentrations of 10.7 mg m^{-3} at a salinity of ~6 vs. 5.6 mg m^{-3} at salinity ~28 on June 27, 2018, and in the range of 33–43 mg m^{-3} for the freshwater samples vs. 4.0 mg m^{-3} at salinity ~29 on June 8, 2018. Longer water residence times at lower discharge can result in significant degradation of allochthonous DOM and stimulate new autochthonous DOM production from localized phytoplankton blooms (i.e., the River Continuum Concept) (Vannote et al., 1980; Paerl et al., 1998; Dixon et al., 2014). Phytoplankton grazing in wetland channels could also be responsible for fluorescence byproducts (Tzortziou et al., 2011), supported by high phaeophytin−*a* in Lord Cove on June 8, 2018 (10.1 mg m^{-3} with Chl-*a* of 11.8 mg m^{-3}).

In both river systems, for the lower river discharge June transects, we found higher C3 F_{max} than C1 and C2 F_{max} in the river endmembers (Fig. 7b, h), consistent with enhanced photochemical transformations under low flow conditions and long residence times (Yoon et al., 2021), especially during summer. In contrast, the April 24, 2019, Housatonic and the May 6, 2021, Connecticut River transects occur during higher discharge periods (spring runoff), and C1 and C2 F_{max} exceed C3 F_{max}, consistent with the Pulse Shunt Concept and export of more humic and less degraded terrigenous organic matter (Raymond et al., 2016). For the higher discharge transects, deviations of $a_{CDOM}(300)$ and DOC from conservative mixing in areas extensively covered by coastal marshes highlight the critical role of wetlands as a source of strongly colored DOC to LIS across a range of environmental and hydrological conditions.

3.4. Drivers of DOM variability across the Sound

PCA allowed us to assess system-wide CDOM variability in LIS further. To do this, it was necessary to analyze CDOM in the context of its environment (D'Andrilli et al., 2022), and therefore, ancillary biogeochemical, physicochemical, and hydrological parameters were incorporated. Samples across the freshwater-to-estuary marine gradient (0 to 35 salinity) were included for PCA, reflecting our understanding of this system as a complicated continuum without definitive endmembers. This is exemplified in Fig. 7, where there is no consistent optical signature of an "endmember" based on salinity because both "ends" are subject to highly variable physical, chemical, and biological conditions.

The first two dimensions from PCA accounted for 47.4 % of the variability (Fig. 6), while the first six dimensions from PCA accounted for 76.0 % of the variability (Table S1), and these dimensions can be attributed to LIS phenomena based on variable coefficient loadings and sample scores. PC1, accounting for most of the observed variability (35.2 %), reveals the transition of terrestrial to marine waters and highlights the importance of discharge-driven gradients as a key driver of CDOM variability across the LIS ecosystem. PC1 has the strongest correlations with salinity, $a_{CDOM}(300)$, $a^*_{CDOM}(300)$, S_R, and $S_{275–295}$ (loadings all ≥0.30) (Fig. 6; Table S1). Like PC1, PC3 shows the importance of freshwater discharge, but PC3 better demonstrates temporal, rather than spatial, controls on LIS hydrology, with positive correlations to Connecticut and Housatonic River discharge and precipitation (loadings all >0.40; Table S1). PC2 represents the seasonal control on LIS, with water temperature having the highest correlation (loading of 0.46; Table S1), and a separation between summer months vs. spring and winter months in sample scores (Fig. 6b).

The first two principal components corresponding to the freshwater-marine continuum and the seasonality for LIS estuary are consistent with findings from Regier et al. (2016), where they explored drivers of DOC fluxes in a subtropical coastal estuary. PCA distilled the most important phenomena contributing to the LIS system-wide surface water variability captured in this study. That six principal components only captured three-quarters of variability suggests dynamism and complexity in this dataset and system. To more explicitly identify the features that control LIS DOC and $a_{CDOM}(300)$, we used multilinear regression models to predict [DOC] and $a_{CDOM}(300)$ in this system. Across all LIS samples from this study (spatiotemporal heterogeneities) ($N = 298$), [DOC] was able to be moderately retrieved ($R^2 = 0.52$) with the statistically significant variables of Chl-*a*, salinity, dissolved oxygen, both river discharges, and precipitation, as well as an interacting term of Chl-*a* with Connecticut River discharge (Table S2). These predictor variables ascertain the allochthonous and autochthonous controls of

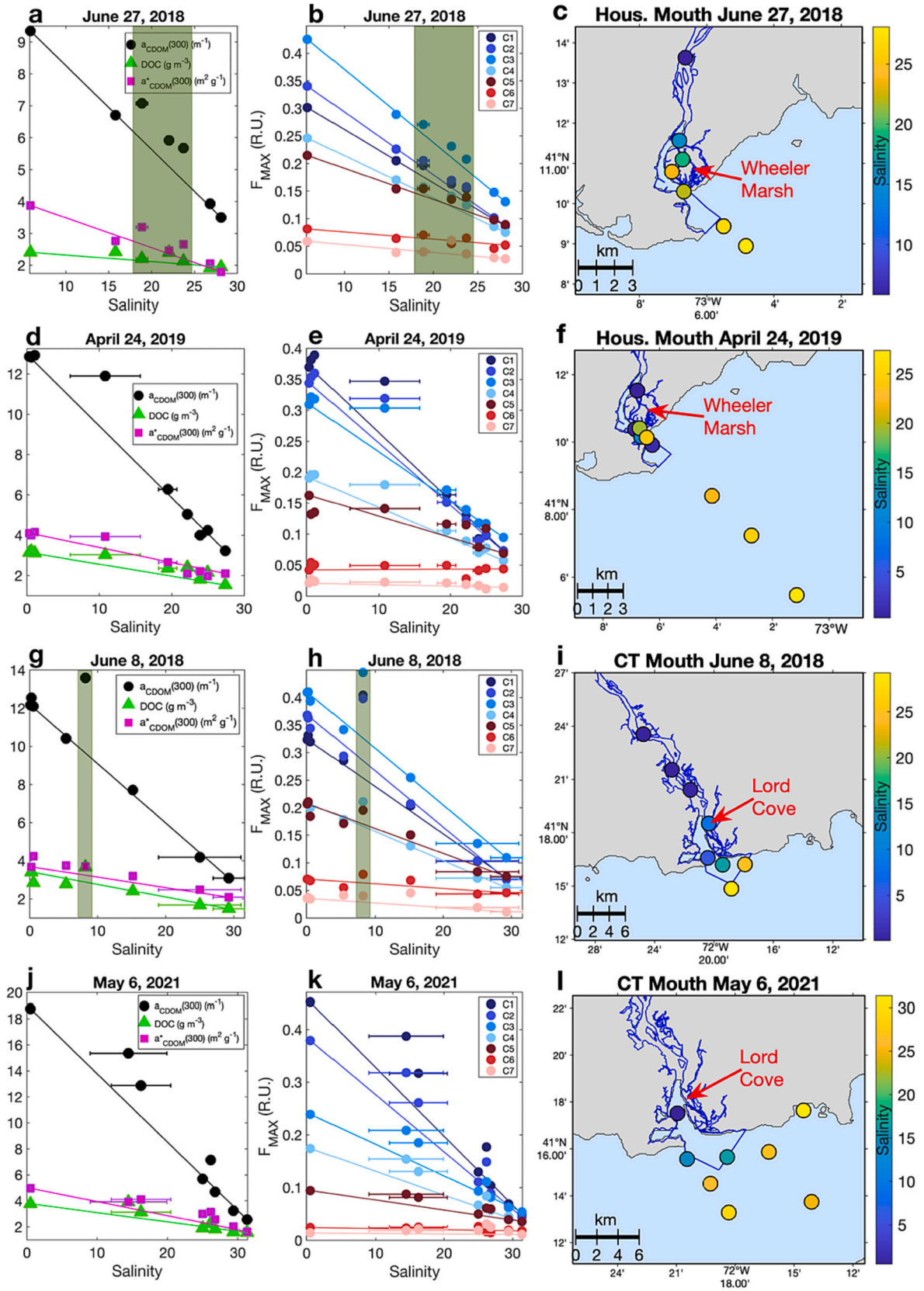

Fig. 7. Selected transects across the Housatonic (a–f) and Connecticut (g–l) Rivers are shown, along with changes in $a_{CDOM}(300)$, [DOC], $a^*_{CDOM}(300)$ (left panel) and component F_{max} (middle panel) across the salinity range. Solid lines connect the freshwater "endmember" to marine "endmember", representing linear conservative mixing with respect to salinity. Horizontal error bars reflect ± one standard deviation for salinity measurements. In the third panel, sample locations, colored by salinity, are shown across the river mouths. Samples taken directly within wetland channels are shaded by the dark green blocks.

DOC in LIS. We were able to strongly predict $a_{CDOM}(300)$ ($R^2 = 0.90$) across space and time in LIS ($N = 298$) using the statistically significant variables of [DOC], salinity, pH, and turbidity, as well as the interacting terms of [DOC] with salinity, and salinity with turbidity (Table S3). The inclusion of pH and turbidity reflect the biological and anthropogenic influences on estuarine CDOM, respectively. Interestingly, [DOC] alone can only moderately ($R^2 = 0.63$) predict $a_{CDOM}(300)$ across LIS.

[DOC] is routinely measured across the main stem of LIS as part of CT DEEP water quality monitoring and is an important biogeochemical parameter with direct ties to carbon cycling and budgets (Vlahos and Whitney, 2017). Together, our measurements of CDOM optical properties and DOC concentrations expand our understanding of DOC quality, source, and fate. For example, a DOC measurement of 2.5 g m^{-3} taken across LIS waters could correspond to $a_{CDOM}(300)$ in the range of ~3.5–10 m^{-1} (Fig. 8). With knowledge of just salinity, it is possible to better constrain the relationship between these two parameters at this higher range of DOC (Fig. 8a). Similarly, for $a_{CDOM}(300)$ with a value of 3.5 m^{-1}, common across all regions of main stem LIS (Fig. 3f–j), C5% would be a strong indicator of higher [DOC] per constant $a_{CDOM}(300)$ (i.e., lower a^*_{CDOM}), indicative of biological DOC production.

4. Summary and conclusions

Comprehensive measurements across the river-estuary continuum over different seasons and multiple years revealed the major drivers of CDOM variability in Long Island Sound, an Estuary of National Significance that is home to >1200 invertebrate species, 170 fish species, and four million people living within its coastal communities (*Long Island Sound Study*). Similar to our results, previous studies showed that freshwater discharge strongly controls temporal biogeochemical variability and trophic status in LIS (Vlahos and Whitney, 2017; Vlahos et al., 2020). Under the most common conditions, LIS is net heterotrophic (i.e., in-situ OM production less than consumption) and a source of (primarily riverine) DOC to the Mid-Atlantic Bight (MAB) (Vlahos and Whitney, 2017). Under relatively low river flow conditions (<19 km^3 yr^{-1}), while still heterotrophic, LIS has been shown to import DOC from the MAB, although more refractory material from rivers may still be exported (Vlahos and Whitney, 2017). However, during exceptionally high river flow conditions (>26 km^3 yr^{-1}), LIS shifts to net autotrophic (i.e., in-situ OM production larger than consumption), and the Eastern LIS becomes a strong source of DOC that is highly enriched by in situ primary production (Vlahos and Whitney, 2017). Water discharge into LIS during the years of this study reached thresholds that imply DOC export and heterotrophic conditions (Vlahos and Whitney, 2017). Lower discharge observed in 2020 (Fig. S2) implies less LIS heterotrophy, but still DOC export to the Mid-Atlantic Bight. Future work should investigate whether our interannual findings from 2020 (lower C3% and higher C4% fluorescence contributions; Fig. 5x, y) are emblematic of a system-wide metabolic response to an altered flow regime.

The integration of CDOM optical measurements with environmental observations in this study allowed us to capture the spatiotemporal heterogeneities of LIS, including its urban-to-rural longitudinal gradient and its dynamic river mouths, across all months of the year and over five years. While carbon-rich and strongly colored terrigenous DOM was dominant in the heavily riverine-influenced Central to Eastern LIS, a clear uncoupling between CDOM absorption and DOC in Western LIS, accompanied by stronger correlations to Chl-*a*, indicated increased marine, or autochthonous, CDOM production. Detailed fluorescence analysis from PARAFAC multi-way decomposition showed clear evidence for seasonal processing of CDOM in LIS, especially increased summertime photochemical degradation of terrestrial humic-like components and shoulder-season microbial processing. The quality of riverine CDOM export was influenced by discharge fluxes, residence time, and coastal wetlands acting as additional sources of strongly humic and colored organic matter. These new and comprehensive in situ measurements allowed us to elucidate the impact of hydrologic, anthropogenic, and biological processes on DOM dynamics and, subsequently, biogeochemical variability and trophic status in this complex urban estuary.

The mechanisms identified from PCA analysis and multilinear regression models that exhibit control on LIS CDOM – freshwater discharge, wastewater inputs, and primary productivity – all are subject to climate change impacts. In LIS, water quality management efforts have focused on reducing nitrogen loads (Save the Sound, 2017). However, there will be a need to reassess our current thresholds for water quality (e.g., from wastewater treatment plants) as LIS faces rising water temperatures and precipitation loads (Staniec and Vlahos, 2017; Whitney and Vlahos, 2021; USGCRP, 2018). Capturing this changing hydrological, biogeochemical, and ecological connectivity of complex urban-riverine-estuarine systems is key for enhanced resource management and policies that promote the maintenance of estuarine functions in the face of increased perturbations and uncertainty.

CRediT authorship contribution statement

Alana Menendez: Writing – review & editing, Writing – original draft, Visualization, Software, Methodology, Investigation, Formal analysis, Data curation, Conceptualization. **Maria Tzortziou:** Writing – review & editing, Writing – original draft, Supervision, Resources, Project administration, Methodology, Investigation, Funding acquisition, Formal analysis, Data curation, Conceptualization.

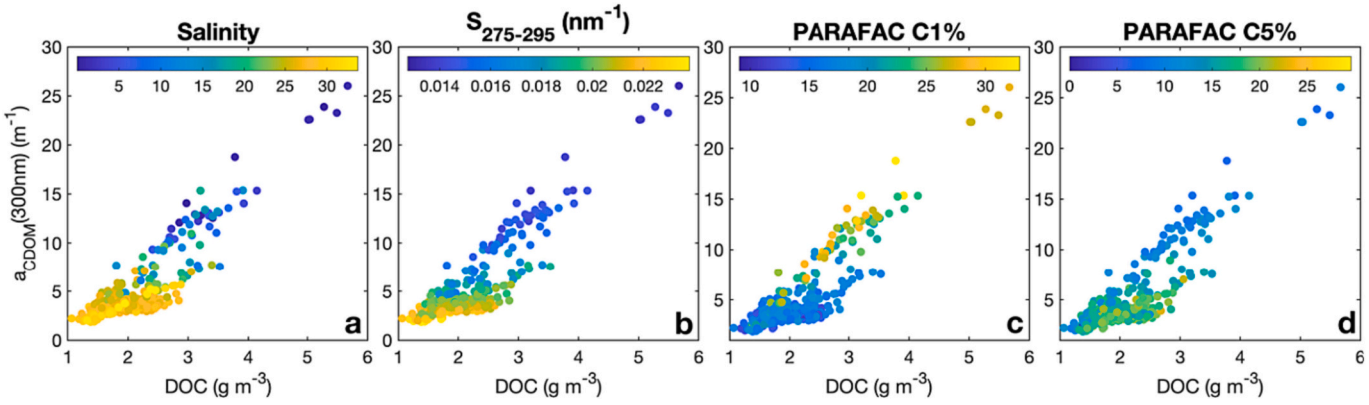

Fig. 8. $a_{CDOM}(300)$ and [DOC] were found to not linearly correlate across the entire study, but instead broadly show a high-salinity, marine, protein-like fork, and a freshwater, terrestrial, humic-like fork.

Declaration of competing interest

The authors declare that they have no known competing financial interests or personal relationships that could have appeared to influence the work reported in this paper.

Data availability

Data will be made available on request.

Acknowledgments

The authors would like to thank Kyle Turner, Brice Grunert, Jonathan Sherman, Tong Lin, Dianne Greenfield, Helga Gomes, Joaquim Goes, and Kali McKee for their contributions with sample collection, data handling, data management, and fieldwork activities. We sincerely thank the Connecticut Department of Energy & Environmental Protection (CT DEEP), including Matt Lyman, Katie O'Brien-Clayton, and Captain Tommy Seda of the *R/V John Dempsey*, for their ongoing collaboration and work to collect valuable long-term data in Long Island Sound. We would like to thank two anonymous reviewers who greatly improved this manuscript.

Funding

This work was supported by National Aeronautics and Space Administration (NASA) grants 80NSSC17K0258 (Interdisciplinary Science Program) and 80NSSC20K1287 (Ocean Biology and Biogeochemistry Program), and EPA/NY and CT Sea Grant (NYSG/CTSG) 82913-1156439. This work was supported and monitored by the National Oceanic and Atmospheric Administration (NOAA) Educational Partnership Program/Minority-Serving Institutions (EPP/MSI) award NA22SEC4810016, Center for Earth System Sciences and Remote Sensing Technologies-II (CESSRST-II). Contents in this manuscript do not reflect the views of NOAA or the U.S. Department of Commerce and solely are representative of the authors. A.M. would like to thank NOAA EPP/MSI and NOAA CESSRST-II for the generous PhD fellowship support.

Appendix A. Supplementary data

Supplementary data to this article can be found online at https://doi.org/10.1016/j.scitotenv.2024.171083.

References

Aiken, G.R., 2014. Fluorescence and dissolved organic matter: a chemist's perspective. In: Coble, P.G., Lead, J., Baker, A., Reynolds, D.M., Spencer, R.G.M. (Eds.), Aquatic Organic Matter Fluorescence. Cambridge University Press, pp. 35–74. https://doi.org/10.1017/CBO9781139045452.005.

Anderson, T.H., Taylor, G.T., 2001. Nutrient pulses, plankton blooms, and seasonal hypoxia in western Long Island sound. Estuaries 24 (2), 228. https://doi.org/10.2307/1352947.

Aurin, D.A., Dierssen, H.M., Twardowski, M.S., Roesler, C.S., 2010. Optical complexity in Long Island Sound and implications for coastal ocean color remote sensing. J. Geophys. Res. Oceans 115 (C7), 1–18. https://doi.org/10.1029/2009JC005837.

Ayad, M., Li, J., Holt, B., Lee, C., 2020. Analysis and classification of stormwater and wastewater runoff from the Tijuana River using remote sensing imagery. Front. Environ. Sci. 8 https://doi.org/10.3389/fenvs.2020.599030.

Bauer, J.E., Cai, W.J., Raymond, P.A., Bianchi, T.S., Hopkinson, C.S., Regnier, P.A.G., 2013. The changing carbon cycle of the coastal ocean. Nature 504 (7478), 61–70. https://doi.org/10.1038/nature.

Blumberg, A.F., Pritchard, D.W., 1997. Estimates of the transport through the East River, New York. J. Geophys. Res. Oceans 102 (C7), 5685–5703. https://doi.org/10.1029/96J C03416.

Boyd, T.J., Osburn, C.L., 2004. Changes in CDOM fluorescence from allochthonous and autochthonous sources during tidal mixing and bacterial degradation in two coastal estuaries. Mar. Chem. 89, 189–210. https://doi.org/10.1016/j.marchem.2004.02.012.

Bricaud, A., Morel, A., Prieur, L., 1981. Absorption by dissolved organic matter of the sea (yellow substance) in the UV and visible domains. Limnol. Oceanogr. 26 (1), 43–53.

Cao, F., Tzortziou, M., 2021. Capturing dissolved organic carbon dynamics with Landsat-8 and Sentinel-2 in tidally influenced wetland–estuarine systems. Sci. Total Environ. 777 https://doi.org/10.1016/j.scitotenv.2021.145910.

Cao, F., Tzortziou, M., 2024. Impacts of hydrology and extreme events on dissolved organic carbon dynamics in a heavily urbanized estuary and its major tributaries: a view from space. JGR-Biogeosciences. https://doi.org/10.1029/2023JG007767.

Cao, F., Tzortziou, M., Hu, C., Mannino, A., Fichot, C.G., Del Vecchio, R., et al., 2018. Remote sensing retrievals of colored dissolved organic matter and dissolved organic carbon dynamics in North American estuaries and their margins. Remote Sens. Environ. 205, 151–165. https://doi.org/10.1016/j.rse.2017.11.014.

Coble, P.G., 1996. Characterization of marine and terrestrial DOM in seawater using excitation-emission matrix spectroscopy. Mar. Chem. 51 (4), 325–346. https://doi.org/10.1016/0304-4203(95) 00062-3.

Cory, R.M., Kling, G.W., 2018. Interactions between sunlight and microorganisms influence dissolved organic matter degradation along the aquatic continuum. Limnol. Oceanogr. Lett. 3 (3), 102–116. https://doi.org/10.1002/lol2.10060.

Cory, R.M., Harrold, K.H., Neilson, B.T., Kling, G.W., 2015. Controls on dissolved organic matter (DOM) degradation in a headwater stream: the influence of photochemical and hydrological conditions in determining light-limitation or substrate-limitation of photo-degradation. Biogeosciences 12 (22), 6669–6685. https://doi.org/10.5194/bg-12-6669-2015.

D'Andrilli, J., Junker, J.R., Smith, H.J., Scholl, E.A., Foreman, C.M., 2019. DOM composition alters ecosystem function during microbial processing of isolated sources. Biogeochemistry 142 (2), 281–298. https://doi.org/10.1007/s10533-018-00534-5.

D'Andrilli, J., Silverman, V., Buckley, S., Rosario-Ortiz, F.L., 2022. Inferring ecosystem function from dissolved organic matter optical properties: a critical review. Environ. Sci. Technol. 56 (16), 11146–11161. https://doi.org/10.1021/acs.est.2c04240.

Deignan-Schmidt, S.R., Whitney, M.M., 2017. A model study on the summertime distribution of river waters in Long Island Sound. Estuar. Coasts 41 (4), 1002–1020. https://doi.org/10.1007/s12237-017-0348-5.

Del Vecchio, R., Blough, N.V., 2002. Photobleaching of chromophoric dissolved organic matter in natural waters: kinetics and modeling. Mar. Chem. 78 (4), 231–253. https://doi.org/10.1016/s0304-4203(02)00036-1.

Del Vecchio, R., Blough, N.V., 2004. Spatial and seasonal distribution of chromophoric dissolved organic matter and dissolved organic carbon in the Middle Atlantic Bight. Mar. Chem. 89 (1–4), 169–187. https://doi.org/10.1016/j.marchem.2004.02.027.

Determann, S., Lobbes, J.M., Reuter, R., Rullkötter, J., 1998. Ultraviolet fluorescence excitation and emission spectroscopy of marine algae and bacteria. Mar. Chem. 62 (1–2), 137–156. https://doi.org/10.1016/s0304-4203(98)00026-7.

Dixon, J.L., Helms, J.R., Kieber, R.J., Avery, G.B., 2014. Biogeochemical alteration of dissolved organic material in the Cape Fear River Estuary as a function of freshwater discharge. Estuar. Coast. Shelf Sci. https://doi.org/10.1016/j.ecss.2014.08.026.

D'Sa, E.J., Tzortziou, M., Liu, B., 2023. Extreme events and impacts on organic carbon cycles from ocean color remote sensing: review with case study, challenges, and future directions. Earth Sci. Rev. 243, 104503 https://doi.org/10.1016/j.earscirev.2023.104503.

Fellman, J.B., D'Amore, D.V., Hood, E., Boone, R.D., 2008. Fluorescence characteristics and biodegradability of dissolved organic matter in forest and wetland soils from coastal temperate watersheds in southeast Alaska. Biogeochemistry 88 (2), 169–184. https://doi.org/10.1007/s10533-008-9203-x.

Fellman, J.B., Hood, E., Spencer, R.G.M., 2010. Fluorescence spectroscopy opens new windows into dissolved organic matter dynamics in freshwater ecosystems: a review. Limnol. Oceanogr. 55 (6), 2452–2462. https://doi.org/10.4319/lo.2010.55.6.2452.

Fichot, C.G., Benner, R., 2011. A novel method to estimate DOC concentrations from CDOM absorption coefficients in coastal waters. Geophys. Res. Lett. 38 (3), 1–5. https://doi.org/10.1029/2010GL046152.

Fichot, C.G., Benner, R., 2012. The spectral slope coefficient of chromophoric dissolved organic matter (S 275-295) as a tracer of terrigenous dissolved organic carbon in river-influenced ocean margins. Limnol. Oceanogr. 57 (5), 1453–1466. https://doi.org/10.4319/lo.2012.57.5.1453.

Fukuzaki, K., Imai, I., Fukushima, K., Ishii, K., Sawayama, S., Yoshioka, T., 2014. Fluorescent characteristics of dissolved organic matter produced by bloom-forming coastal phytoplankton. J. Plankton Res. 36 (3), 685–694. https://doi.org/10.1093/plankt/fbu015.

Gay, P., O'Donnell, J., 2009. Comparison of the salinity structure of the Chesapeake Bay, the Delaware Bay and Long Island Sound using a linearly tapered advection-dispersion model. Estuaries Coasts 32, 68–87. https://doi.org/10.1007/s12237-008-9101-4.

Grunert, B., Tzortziou, M., Neale, P.J., Menendez, A., Hernes, P.J., 2021. DOM degradation by light and microbes along the Yukon River-coastal ocean continuum. Sci. Rep. 11 (1) https://doi.org/10.1038/s41598-021-89327-9.

Helms, J.R., Stubbins, A., Ritchie, J.D., Minor, E.C., Kieber, D.J., Mopper, K., 2008. Absorption spectral slopes and slope ratios as indicators of molecular weight, source, and photobleaching of chromophoric dissolved organic matter. Limnol. Oceanogr. 53 (3), 955–969. https://doi.org/10.4319/lo.2008.53.3.0955.

Hernes, P.J., Benner, R., 2003. Photochemical and microbial degradation of dissolved lignin phenols: implications for the fate of terrigenous dissolved organic matter in marine environments. J. Geophys. Res. Oceans 108 (C9). https://doi.org/10.1029/2002jc001421.

Humphries, G.E., Espinosa, J.I., Ambrosone, M., Ayala, Z.R., Tzortziou, M., Goés, J.I., Greenfield, D.I., 2023. Transitions in nitrogen and organic matter form and concentration correspond to bacterial population dynamics in a hypoxic urban estuary. Biogeochemistry 163, 219–243. https://doi.org/10.1007/s10533-023-01021-2.

Ishii, S.K., Boyer, T.H., 2012. Behavior of reoccurring PARAFAC components in fluorescent dissolved organic matter in natural and engineered systems: a critical review. Environ. Sci. Technol. 46 (4), 2006–2017. https://doi.org/10.1021/es2043504.

Joshi, I.D., D'Sa, E.J., Osburn, C.L., Bianchi, T.S., Ko, D.S., Oviedo-Vargas, D., Arellano, A.R., Ward, N.D., 2017. Assessing chromophoric dissolved organic matter (CDOM) distribution, stocks, and fluxes in Apalachicola Bay using combined field, viirs ocean color, and model observations. Remote Sens. Environ. 191, 359–372. https://doi.org/10.1016/j.rse.2017.01.039.

Judd, K.E., Crump, B.C., Kling, G.W., 2006. Variation in dissolved organic matter controls bacterial production and community composition. Ecology 87 (8), 2068–2079. https://doi.org/10.1890/0012-9658(2006)87.

Juhls, B., Overduin, P.P., Hölemann, J., Hieronymi, M., Matsuoka, A., Heim, B., Fischer, J., 2019. Dissolved organic matter at the fluvial–marine transition in the Laptev Sea using in situ data and ocean colour remote sensing. Biogeosciences 16, 2693–2713. https://doi.org/10.5194/bg-16-2693-2019.

Kim, G.E., Gnanadesikan, A., Pradal, M.A., 2016. Increased surface ocean heating by colored detrital matter (CDM) linked to greater Northern Hemisphere ice formation in the GFDL CM2MC ESM. J. Climate 29 (24), 9063–9076. https://doi.org/10.1175/jcli-d-16-0053.1.

Kothawala, D.N., Stedmon, C.A., Müller, R.A., Weyhenmeyer, G.A., Köhler, S.J., Tranvik, L.J., 2014. Controls of dissolved organic matter quality: evidence from a large-scale boreal lake survey. Glob. Chang. Biol. 20 (4), 1101–1114. https://doi.org/10.1111/gcb.12488.

Lakowicz, J.R., 2006. Principles of Fluorescence Spectroscopy, 3rd ed. Springer.

Lee, Y., Lwiza, K.M.M., 2008. Characteristics of bottom dissolved oxygen in Long Island Sound, New York. Estuarine Coast. Shelf Sci. 76 (2), 187–200. https://doi.org/10.1016/j.ecss.2007. 07.001.

Logozzo, L., Tzortziou, M., Neale, P., Clark, J.B., 2021. Photochemical and microbial degradation of chromophoric dissolved organic matter exported from tidal marshes. J. Geophys. Res. Biogeosci. 126 (4) https://doi.org/10.1029/2020JG005744.

Maie, N., Scully, N.M., Pisani, O., Jaffé, R., 2007. Composition of a protein-like fluorophore of dissolved organic matter in coastal wetland and estuarine ecosystems. Water Res. 41 (3), 563–570. https://doi.org/10.1016/j.watres.2006.11.006.

Mann, P., Davydova, A.I., Zimov, S.A., Spencer, R.G.M., Davydov, S., Bulygina, E.B., Holmes, R.M., 2012. Controls on the composition and lability of dissolved organic matter in Siberia's Kolyma River basin. J. Geophys. Res. Biogeosci. 117 (G1) https://doi.org/10.1029/2011jg001798.

Mannino, A., Russ, M.E., Hooker, S.B., 2008. Algorithm development and validation for satellite-derived distributions of DOC and CDOM in the U.S. Middle Atlantic Bight. J. Geophys. Res. Oceans 113 (7), 1–19. https://doi.org/10.1029/2007JC004493.

McKnight, D.M., Boyer, E.W., Westerhoff, P., Doran, P.T., Kulbe, T., Andersen, D.T., 2001. Spectrofluorometric characterization of dissolved organic matter for indication of precursor organic material and aromaticity. Limnol. Oceanogr. 46 (1), 38–48. https://doi.org/10.4319/lo.2001.46.1.0038.

Menden-Deuer, S., Montalbano, A.L., 2015. Bloom formation potential in the harmful dinoflagellate Akashiwo sanguinea: clues from movement behaviors and growth characteristics. Harmful Algae 47, 75–85. https://doi.org/10.1016/j.hal.2015.06.001.

Menendez, A., Tzortziou, M., Neale, P.J., Megonigal, J.P., Powers, L.C., Schmitt-Kopplin, P., Gonsior, M., 2022. Strong dynamics in tidal marsh DOC export in response to natural cycles and episodic events from continuous monitoring. J. Geophys. Res. Biogeosci. 127 (7) https://doi.org/10.1029/2022jg006863.

Murphy, K.R., Stedmon, C.A., Waite, T.D., Ruiz, G.M., 2008. Distinguishing between terrestrial and autochthonous organic matter sources in marine environments using fluorescence spectroscopy. Mar. Chem. 108 (1–2), 40–58. https://doi.org/10.1016/j.marchem.2007.10.003.

Murphy, K.R., Stedmon, C.A., Graeber, D., Bro, R., 2013. Fluorescence spectroscopy and multi-way techniques. PARAFAC. Anal. Methods 5 (23), 6557. https://doi.org/10.1039/c3ay41160e.

Murphy, K.R., Stedmon, C.A., Wenig, P., Bro, R., 2014. OpenFluor – an online spectral library of auto-fluorescence by organic compounds in the environment. Anal. Methods 6, 658–661. https://doi.org/10.1039/c3ay41935e.

Najjar, R.G., Herrmann, M., Alexander, R., Boyer, E.W., Burdige, D.J., Butman, D., et al., 2018. Carbon budget of tidal wetlands, estuaries, and shelf waters of Eastern North America. Global Biogeochem. Cycles 32 (3), 389–416. https://doi.org/10.1002/2017GB005790.

Nelson, N.B., Siegel, D.A., 2002. Chromophoric DOM in the open ocean. In: Hansell, D. A., Carlson, C.A. (Eds.), Biogeochemistry of Marine Dissolved Organic Matter. Academic Press, pp. 547–578.

Nelson, N.B., Carlson, C.A., Steinberg, D.K., 2004. Production of chromophoric dissolved organic matter by Sargasso Sea microbes. Mar. Chem. 89 (1–4), 273–287. https://doi.org/10.1016/j.marchem.2004.02.017.

Omori, Y., Saeki, A., Wada, S., Inagaki, Y., Hama, T., 2020. Experimental analysis of diurnal variations in humic-like fluorescent dissolved organic matter in surface seawater. Front. Mar. Sci. 7 https://doi.org/10.3389/fmars.2020.589064.

Paerl, H.W., Pinckney, J.L., Fear, J.M., Peierls, B.L., 1998. Ecosystem responses to internal and watershed organic matter loading: consequences for hypoxia in the eutrophying Neuse River Estuary, North Carolina, USA. Mar. Ecol. Prog. Ser. 166, 17–25. https://doi.org/10.3354/meps166017.

Raymond, P.A., Bauer, J.E., 2001. DOC cycling in a temperate estuary: a mass balance approach using natural 14C and 13C isotopes. Limnol. Oceanogr. 46 (3), 655–667. https://doi.org/10.4319/lo.2001.46.3.0655.

Raymond, P.A., Saiers, J.E., Sobczak, W.V., 2016. Hydrological and biogeochemical controls on watershed dissolved organic matter transport: pulse-shunt concept. Ecology 97 (1), 5–16. https://doi.org/10.1890/14-1684.1.

Regier, P., Briceño, H., Jaffé, R., 2016. Long-term environmental drivers of DOC fluxes: linkages between management, hydrology and climate in a subtropical coastal estuary. Estuar. Coast. Shelf Sci. 182, 112–122. https://doi.org/10.1016/j.ecss.2016.09.017.

Regnier, P., Resplandy, L., Najjar, R.G., Ciais, P., 2022. The land-to-ocean loops of the global carbon cycle. Nature 603 (7901), 401–410. https://doi.org/10.1038/s41586-021-04339-9.

Rice, E.J., Stewart, G., 2013. Analysis of interdecadal trends in chlorophyll and temperature in the Central Basin of Long Island Sound. Estuar. Coast. Shelf Sci. 128, 64–75. https://doi.org/10.1016/j.ecss.2013.05.002.

Romera-Castillo, C., Sarmento, H., Álvarez-Salgado, X.A., Gasol, J.M., Marrasé, C., 2009. Production of chromophoric dissolved organic matter by marine phytoplankton. Limnol. Oceanogr. 55 (1), 446–454. https://doi.org/10.4319/lo.2010.55.1.0446.

Romera-Castillo, C., Sarmento, H., Alvarez-Salgado, X.A.Á., Gasol, J.M., Marrasé, C., 2011. Net production and consumption of fluorescent colored dissolved organic matter by natural bacterial assemblages growing on marine phytoplankton exudates. Appl. Environ. Microbiol. 77 (21), 7490–7498. https://doi.org/10.1128/AEM.00200-11.

Sanwlani, N., Evans, C.D., Müller, M., Cherukuru, N., Martin, P., 2022. Rising dissolved organic carbon concentrations in coastal waters of northwestern Borneo related to tropical peatland conversion. Sci. Adv. 8 (15) https://doi.org/10.1126/sciadv.abi5688.

Save the Sound, 2017. New York City Nitrogen Report: East River and Long Island Sound. https://www.savethesound.org/wp-content/uploads/2018/03/NYC-Nitrogen-Report-East-River.pdf.

Save the Sound, 2022. Long Island Sound Report Card. https://www.savethesound.org/report-card.

Scully, N.M., Maie, N., Dailey, S.K., Boyer, J.N., Jones, R.D., Jaffé, R., 2004. Early diagenesis of plant-derived dissolved organic matter along a wetland, mangrove, estuary ecotone. Limnol. Oceanogr. 49 (5), 1667–1678. https://doi.org/10.4319/lo.2004.49.5.1667.

Sherman, J., Tzortziou, M., Turner, K.J., Goes, J.I., Grunert, B., 2023a. Chlorophyll dynamics from Sentinel-3 using an optimized algorithm for enhanced ecological monitoring in complex urban estuarine waters. Int. J. Appl. Earth Obs. Geoinf. 118, 103223 https://doi.org/10.1016/j.jag.2023.103223.

Sherman, J., Tzortziou, M., Turner, K.J., Greenfield, D.I., Menendez, A., 2023b. Deciphering the water quality impacts of COVID-19 human mobility shifts in estuaries surrounding New York City. Sci. Total Environ. 896, 164953 https://doi.org/10.1016/j.scitotenv.2023.164953.

Shimotori, K., Omori, Y., Hama, T., 2009. Bacterial production of marine humic-like fluorescent dissolved organic matter and its biogeochemical importance. Aquat. Microb. Ecol. 58, 55–66. https://doi.org/10.3354/ame01350.

Staniec, A., Vlahos, P., 2017. Timescales for determining temperature and dissolved oxygen trends in the Long Island Sound (LIS) estuary. Cont. Shelf Res. 151, 1–7. https://doi.org/10.1016/j.csr.2017.09.013.

Stedmon, C.A., Markager, S., 2005. Resolving the variability in dissolved organic matter fluorescence in a temperate estuary and its catchment using PARAFAC analysis. Limnol. Oceanogr. 50 (2), 686–697. https://doi.org/10.4319/lo.2005.50.2.0686.

Stedmon, C., Nelson, N.B., 2015. The optical properties of DOM in the ocean. In: Hansell, D.A., Carlson, C.A. (Eds.), Biogeochemistry of Marine Dissolved Organic Matter, 2. ed. Elsevier, pp. 481–508.

Stedmon, C.A., Markager, S., Kaas, H., 2000. Optical properties and signatures of chromophoric dissolved organic matter (CDOM) in Danish coastal waters. Estuar. Coast. Shelf Sci. 51 (2), 267–278. https://doi.org/10.1006/ecss.2000.0645.

Stedmon, C.A., Markager, S., Bro, R., 2003. Tracing dissolved organic matter in aquatic environments using a new approach to fluorescence spectroscopy. Mar. Chem. 82 (3–4), 239–254. https://doi.org/10.1016/s0304-4203(03)00072-0.

Stedmon, C.A., Markager, S., Tranvik, L.J., Kronberg, L., Slätis, T., Martinsen, W., 2007. Photochemical production of ammonium and transformation of dissolved organic matter in the Baltic Sea. Mar. Chem. 104 (3–4), 227–240. https://doi.org/10.1016/j.marchem.2006.11.005.

Steinberg, D., Nelson, N., Carlson, C., Prusak, A., 2004. Production of chromophoric dissolved organic matter (CDOM) in the open ocean by Zooplankton and the colonial cyanobacterium Trichodesmium spp. Mar. Ecol. Prog. Ser. 267, 45–56. https://doi.org/10.3354/meps267045.

Stubbins, A., Lapierre, J., Berggren, M., Prairie, Y.T., Dittmar, T., Del Giorgio, P.A., 2014. What's in an EEM? Molecular signatures associated with dissolved organic fluorescence in boreal Canada. Environ. Sci. Technol. 48 (18), 10598–10606. https://doi.org/10.1021/es502086e.

Supino, J.R., 2020. Microbial Degradability of Terrigenous, Marsh-Exported, and Estuarine Colored Dissolved Organic Matter in Long Island Sound (MSc Thesis). CUNY Academic Works.

Tzortziou, M., Subramaniam, A., Herman, J.R., Gallegos, C.L., Neale, P.J., Harding, L.W., 2007. Remote sensing reflectance and inherent optical properties in the mid Chesapeake Bay. Estuarine Coast. Shelf Sci. 72 (1–2), 16–32. https://doi.org/10.1016/j.ecss.2006.09.018.

Tzortziou, M., Neale, P.J., Osburn, C.L., Megonigal, J.P., Maie, N., Jaffé, R., 2008. Tidal marshes as a source of optically and chemically distinctive colored dissolved organic matter in the Chesapeake Bay. Limnol. Oceanogr. 53 (1), 148–159. https://doi.org/10.4319/lo.2008.53.1.0148.

Tzortziou, M., Neale, P.J., Megonigal, J.P., Pow, C.L., Butterworth, M., 2011. Spatial gradients in dissolved carbon due to tidal marsh outwelling into a Chesapeake Bay estuary. Mar. Ecol. Prog. Ser. 426, 41–56. https://doi.org/10.3354/meps09017.

USGCRP, 2018. In: Reidmiller, D.R., Avery, C.W., Easterling, D.R., Kunkel, K.E., Lewis, K.L.M., Maycock, T.K., Stewart, B.C. (Eds.), Impacts, Risks, and Adaptation in the United States: Fourth National Climate Assessment, volume II. U.S. Global Change

Research Program, Washington, DC, USA. https://doi.org/10.7930/NCA4.2018, 1515 pp.
Valle-Levinson, A., Wilson, R.E., Swanson, R.L., 1995. Physical mechanisms leading to hypoxia and anoxia in Western Long Island Sound. Environ. Int. 21 (5), 657–666. https://doi.org/10.1016/0160-4120(95)00076-w.
Vannote, R.L., Minshall, G.W., Cummins, K.W., Sedell, J.R., Cushing, C.E., 1980. The river continuum concept. Can. J. Fish. Aquat. Sci. 37 (1), 130–137. https://doi.org/10.1139/f80-017.
Vantrepotte, V., Danhiez, F.-P., Loisel, H., Ouillon, S., Mériaux, X., Cauvin, A., Dessailly, D., 2015. CDOM-DOC Relationship in contrasted coastal waters: Implication for doc retrieval from Ocean Color Remote Sensing Observation. Opt. Express 23 (1), 33. https://doi.org/10.1364/oe.23.000033.
Vaudrie, J., 2017. New York City's impact on Long Island Sound water quality technical report. In: Save the Sound. https://vaudrey.lab.uconn.edu/wp-content/uploads/sites/1663/2018/07/2017-11-16-Vaudrey-NYC-N.pdf.
Vlahos, P., Whitney, M.M., 2017. Organic carbon patterns and budgets in the Long Island Sound estuary. Limnol. Oceanogr. 62 (S1) https://doi.org/10.1002/lno.10638.
Vlahos, P., Whitney, M.M., Menniti, C., Mullaney, J.R., Morrison, J., Jia, Y., 2020. Nitrogen budgets of the Long Island Sound estuary. Estuarine Coast. Shelf Sci. 232, 106493 https://doi.org/10.1016/j.ecss.2019.106493.
Vodacek, A., Blough, N.V., DeGrandpre, M.D., Nelson, R.K., 1997. Seasonal variation of CDOM and DOC in the Middle Atlantic Bight: terrestrial inputs and photooxidation. Limnol. Oceanogr. 42 (4), 674–686. https://doi.org/10.4319/lo.1997.42.4.0674.
Ward, N.D., Megonigal, J.P., Bond-Lamberty, B., Bailey, V., Butman, D., Canuel, E.A., et al., 2020. Representing the function and sensitivity of coastal interfaces in Earth system models. Nat. Commun. 11 (1) https://doi.org/10.1038/s41467-020-16236-2.
Whitney, M.M., Vlahos, P., 2021. Reducing hypoxia in an urban estuary despite climate warming. Environ. Sci. Technol. 55 (2), 941–951. https://doi.org/10.1021/acs.est.0c03964.
Wünsch, U., Murphy, K.R., Stedmon, C.A., 2015. Fluorescence quantum yields of natural organic matter and organic compounds: implications for the fluorescence-based interpretation of organic matter composition. Front. Mar. Sci. 2 https://doi.org/10.3389/fmars.2015.00098.
Xiao, X., Powers, L.C., Liu, J., Gonsior, M., Zhang, R., Zhang, L., et al., 2022. Biodegradation of terrigenous organic matter in a stratified large-volume water column: implications of the removal of terrigenous organic matter in the Coastal Ocean. Environ. Sci. Technol. 56 (8), 5234–5246. https://doi.org/10.1021/acs.est.1c08317.
Yamashita, Y., Tanoue, E., 2003. Chemical characterization of protein-like fluorophores in DOM in relation to aromatic amino acids. Mar. Chem. 82 (3–4), 255–271. https://doi.org/10.1016/s 0304-4203(03)00073-2.
Yamashita, Y., Tanoue, E., 2004. In situ production of chromophoric dissolved organic matter in coastal environments. Geophys. Res. Lett. 31 (14) https://doi.org/10.1029/2004gl019734.
Yamashita, Y., Nosaka, Y., Suzuki, K., Ogawa, H., Takahashi, K., Saito, H., 2013. Photobleaching as a factor controlling spectral characteristics of chromophoric dissolved organic matter in open ocean. Biogeosciences 10, 7207–7217. https://doi.org/10.5194/bg-10-7207-2013.
Yoon, B., Hosen, J.D., Kyzivat, E.D., Fair, J.H., Weber, L., Aho, K.S., et al., 2021. Export of photolabile and photoprimable dissolved organic carbon from the Connecticut River. Aquat. Sci. 83 (2) https://doi.org/10.1007/s00027-021-00778-8.
Zangrando, R., Corami, F., Barbaro, E., Grosso, A., Barbante, C., Turetta, C., et al., 2019. Free phenolic compounds in waters of the Ross Sea. Sci. Total Environ. 650, 2117–2128. https://doi.org/10.1016/j.scitotenv.2018.09.360.
Zhang, Y., Gao, X., Guo, W., Zhao, J., Li, Y., 2018. Origin and dynamics of dissolved organic matter in a mariculture area suffering from summertime hypoxia and acidification. Front. Mar. Sci. 5 https://doi.org/10.3389/fmars.2018.00325.